INSTITUTE OF PHYSICS PUBLISHING MEASUREMENT SCIENCE AND TECHNOLOGY

Meas. Sci. Technol. **17** (2006) R37–R54 doi:10.1088/0957-0233/17/4/R01

REVIEW ARTICLE

Scintillation detectors for x-rays

Martin Nikl

Institute of Physics, Academy of Sciences of the Czech Republic, Cukrovarnicka 10, 162 53 Prague, Czech Republic

Received 23 March 2005
Published 10 February 2006
Online at stacks.iop.org/MST/17/R37

Abstract
Recent research in the field of phosphor and scintillator materials and related detectors is reviewed. After a historical introduction the fundamental issues are explained regarding the interaction of x-ray radiation with a solid state. Crucial parameters and characteristics important for the performance of these materials in applications, including the employed measurement methods, are described. Extended description of the materials currently in use or under intense study is given. Scintillation detector configurations are further briefly overviewed and selected applications are mentioned in more detail to provide an illustration.

Keywords: luminescence intensity, luminescence kinetics, light detection, x-ray detection, scintillators, phosphors, traps and material imperfections

(Some figures in this article are in colour only in the electronic version)

1. Introduction

It was 110 years ago in November 1895 that Wilhelm Conrad Roentgen noticed the glow of a barium platino-cyanide screen, placed next to his operating discharge tube, and discovered new invisible and penetrating radiation [1], which was named x-ray in English or 'Roentgen radiation' in some other languages. In the x-ray registration a simple photographic film was found rather inefficient and the search for materials to convert x-rays to visible light started immediately to couple them with sensitive photographic film-based detectors. Pupin introduced $CaWO_4$ powder[1], which was used for this purpose for more than 75 years. Together with ZnS-based powders introduced a few years later by Crookes and Regener, $CaWO_4$ powder constitutes the longest-in-use so-called phosphor material employed for the detection of x-rays. It is interesting to note that in 1897 the cathode ray tube (CRT) was invented by Braun, in which the energy of an accelerated electron beam is converted into visible light (called cathodoluminescence) by a phosphor material. The mechanism of this conversion is quite similar [2] to that functioning in the case of x-ray conversion. Thus, at the end of the 19th century, two energetic, photon and particle radiations were available and their enormous application potential forced strongly the development of phosphor and scintillator materials to be used in their exploitation.

It is to be noticed that for registration of x-ray the so-called direct registration principle is widely used, in which the incoming radiation is directly converted into electrical current in a semiconducting material. However, this concept is outside the scope of this work. Moreover, description of materials is restricted to the crystalline wide band-gap solid state ones due to the extremely wide variety of materials also used for the scintillation detection, e.g. plastic, glass materials, liquids or pressurized gases are not included in this work.

Due to the high practical importance and relatively long history of this field, there already exists a large amount of published information on this topic. Let us mention at the beginning the superb recent survey of luminescent materials written by Blasse and Grabmaier [3], the overview of methodology in use in radiation measurement authored by Knoll [4], the recent monograph devoted to scintillator materials from Rodnyi [5] and the useful phosphor handbook written by Shionoya and Yen [6] followed by the more recent and technologically oriented successor from Yen and Weber [7]. Numerous featured review papers on phosphor and scintillator materials and their applications exist in the scientific literature as well, for instance [8–13].

It is the aim of this paper to provide an insight into this topic for a wider scientific audience and at the same

[1] Mentioned also by T A Edison in Notes, *Nature* **53** 470 (1896).

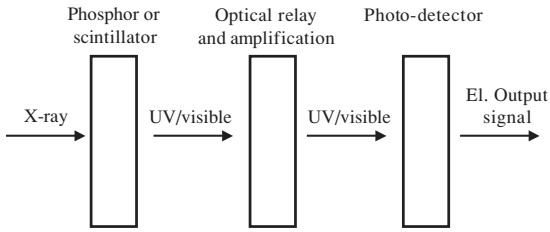

Figure 1. A sketch of a scintillation detector with the main constituent parts.

time review some current hot topics in this field. After reviewing the fundamental physical processes of the x-to-visible light transformation occurring in crystalline phosphor and scintillator materials, practically important material parameters, characteristics and related measurement principles will be summarized. After that an overview of powder, optical ceramics and single crystal materials employed or researched for this purpose will be given. Configurations of scintillation detectors will be further sketched and finally selected applications will be briefly described.

2. Fundamentals

Scintillation detectors consist of a scintillator (phosphor) material followed by an optional optical relay element and a photodetector (figure 1). After an x- or γ-ray photon absorption the ultraviolet/visible light arises in scintillator conversion, which is focused (sometimes also further amplified) by the optical relay element onto the photodetector at the output of which an electrical signal is available for further processing.

2.1. Scintillation conversion mechanism

Wide band-gap materials are employed for transformation of the x-ray to ultraviolet/visible photons. Consistent phenomenological descriptions of the scintillation conversion process, efficiency criteria, etc were developed in the seventies [14] and further refined later [15]. Scintillation conversion is a relatively complicated issue, which can be divided into three consecutive sub-processes—*conversion, transport* and *luminescence* (figure 2). During the initial conversion a multi-step interaction of a high-energy (here considered below ∼1 MeV) photon with the lattice of the scintillator material occurs through the photoelectric effect and Compton scattering effect; below 100 keV photon energy the former is of major importance. Many electron–hole pairs are created and thermalized in the conduction and valence bands, respectively. This first stage is concluded within less than 1 ps. More detailed considerations about the conversion processes have been published in [16, 17]. In the transport process, electrons and holes (eventually created excitons) migrate through the material, repeated trapping at defects may occur, energy losses are probable due to nonradiative recombination, etc. Considerable delay in the migration can be introduced due to the mentioned charge carrier recapture at trapping levels in the material forbidden gap. This stage is the least predictable as material point defects, flaws, surfaces and interfaces can introduce energy levels into the forbidden

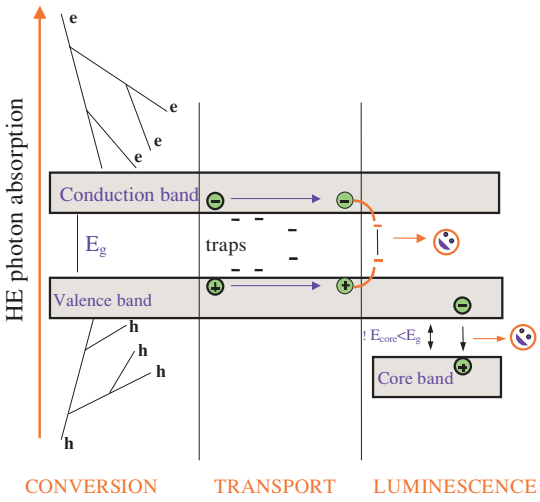

Figure 2. A sketch of the scintillator conversion mechanism in a wide band-gap single crystal solid state. The process is divided into three consecutive stages of conversion, transport and luminescence, which are described in the text.

gap and strongly modify/degrade otherwise high intrinsic scintillation performance. Apparently these phenomena are strongly manufacturing technology dependent [18]. The final stage, luminescence, consists in consecutive trapping of the electron and hole at the luminescence centre and their radiative recombination. In a particular group of materials the light generation occurs in radiative transitions between the valence and first core bands as sketched in figure 2; these are so-called cross-luminescence scintillators [5]. The latter mechanism enables very fast, even subnanosecond, scintillation response, which is, however, usually accompanied by much slower exciton-related luminescence. It is reported in the literature mainly for BaF_2 and other halide single crystals [19]. The physics of luminescent centres is usually well understood due to advanced experimental methods available for their selective and time-resolved study, see e.g. [3, 4].

2.2. Material characteristics and measurement principles

As mentioned in the introduction, in the early days of x-ray usage, just the phosphor powders in the form of thin screens were employed for their registration, coupled together with a photographic film [8]. Later on, due to the need to detect and monitor also higher energy x- or γ-rays, true bulky scintillator materials were introduced in the form of single crystals, namely Tl-doped NaI and CsI single crystals [20, 21], which were the first materials developed for this purpose at the end of forties and have been widely used up to the present day due to their high scintillation efficiency.

Despite the fact that the underlying physics is identical, scientific communities working on phosphors and scintillators have been partially separated, mainly due to the different demands of related applications and different preparation technologies employed [7–9]. Commonly, materials are called phosphors when used in the applications using photon integrating (steady-state) mode detection, while scintillators are employed in the (x- or γ-ray) photon counting regime. Today, the separation between phosphor (powders) and scintillator (bulky solid state) materials somewhat diminishes

as some of the materials are used in both detection modes, in powder or bulky or other forms, depending on the application.

2.2.1. Material characteristics and parameters. In the case of phosphors, their major use is in phosphor screens where a thin layer of phosphor is used to convert an x-ray image into a light one using a defined and stable x-ray source. Their most frequently considered characteristics are as follows:

(1) overall efficiency of x-ray-to-light conversion,
(2) x-ray stopping power,
(3) luminescence decay time and afterglow (persistence),
(4) spectral matching between the phosphor emission spectrum and photo-detector,
(5) chemical stability and radiation resistance,
(6) linearity of light response with incident x-ray dose and intensity and
(7) spatial resolution across the screen.

In the case of scintillators, x(γ)-ray photon counting consists of accumulating the generated light arriving soon after the initial conversion stage is accomplished (figure 2), i.e. strongly delayed light, e.g. due to retrapping processes mentioned above, is of no use. Also x(γ)-ray photons of different energy should be resolved in some applications. The most important characteristics are as follows:

(1) light yield,
(2) x-ray stopping power,
(3) scintillation response—decay time,
(4) spectral matching between the scintillator emission spectrum and photo-detector,
(5) chemical stability and radiation resistance and
(6) linearity of light response with the incident x(γ)-ray photon energy—energy resolution.

While the parameters in (2), (4) and (5) are the same for both phosphor and scintillator materials, different requirements reflected in the other ones are dictated by the detection mode (photon integrating or counting) and the applications themselves.

The overall efficiency of x-ray-to-light conversion considered in phosphors is determined both by intrinsic and extrinsic material characteristics. For the number of UV/visible photons N_{ph} produced in the scintillation conversion per energy E of incoming x(γ)-ray photon an equation was derived [14–16] as follows:

$$N_{ph} = \{E/(\beta E_g)\}SQ \tag{1}$$

where E_g stands for the material forbidden gap, S and Q are quantum efficiencies of the transport and luminescence stages and phenomenological parameter β was found to be between 2 and 3 for most materials. Relative efficiency can then be obtained as

$$\eta = E_{vis}N_{ph}/E, \tag{2}$$

where E_{vis} stands for the energy of generated UV/vis photons. The most efficient material among the phosphors and scintillators today is ZnS:Ag with $\eta \sim 0.2$. If we consider that the forbidden gap of all these materials is $E_g > 3$ eV, it appears improbable that more efficient materials could be found.

Light yield considered for scintillators is an analogue of the overall conversion efficiency in phosphors, but always shows an inferior value in terms of equation (1) as it represents the fraction of generated visible photons, which arrived at the photo-detector within a certain time gate after the high-energy photon absorption; typical values of such a time gate are in practice set between 100 ns and 10 μs.

The x-ray stopping power (attenuation coefficient) of a given thickness of a material depends on its density ρ and effective atomic number Z_{eff}, for the calculation of Z_{eff}, see e.g. [9]. Considering only the interaction through the photoelectric effect the x-ray stopping power appears proportional to ρZ_{eff}^{3-4} [13].

The kinetics of the light response of a phosphor or scintillator is clearly given by the characteristics of the transport and luminescence stages in figure 2 as they are by far slower with respect to the initial conversion. The decay rate of the luminescence centre itself is defined by its transition dipole moment from the excited-to-ground state and can be further enhanced by additional nonradiative quenching, or energy transfer processes away from the excited state. Such quenching or energy transfer, however, results in the decrease of parameter Q in equation (1) and the overall conversion efficiency gets smaller. In the simplest case of exponential decay, the emission intensity $I(t)$ is

$$I(t) \sim \exp[-t/\tau] \tag{3}$$

and τ is called the decay time. While for the parity and/or spin forbidden transitions for most of the rare earth ions decay times are typically of the order of several tens of μs up to ms, in the case of allowed 5d–4f transitions of Ce^{3+} and Pr^{3+} the values scale down to tens of ns and fully allowed singlet–singlet transitions in organic molecules are still about ten times faster. The fastest emission transitions are offered by the radiative decay of Wannier excitons in direct gap semiconductors, where subnanosecond values were reported for compounds such as ZnO, CuX, $CsPbX_3$ (X = Cl, Br), PbI_2, HgI_2, etc. The emission rate is enabled by the coherent character of the exciton state spread over a (large) number of elementary cells [22]. However, a serious disadvantage of the latter group of materials consists in their lower binding energy of related excitonic state, which results in partial ionization and consequently quenching of the exciton-related emission at room temperature and further efficiency decrease follows in bulky elements from the small Stokes shift, which leads to noticeable reabsorption losses.

Due to the mentioned retrapping processes during the transport stage sketched in figure 2, the light response of a material under high-energy excitation is often further complicated by slower non-exponential components. In the case of phosphors, these processes are currently quantified by the afterglow (sometimes called persistence), which is defined as a residual light intensity at some time (typically a few ms) after the excitation is cut off, see [18, 23]. In scintillator decay, such processes are less followed, even if they clearly lower the value of light yield [24] and also signal-to-background ratio is worsened. In some studies a so-called parameter alpha was introduced to provide a comparative measure for the occurrence of delayed radiative recombination within tens to hundreds of μs time scale [10, 25, 26], which is illustrated

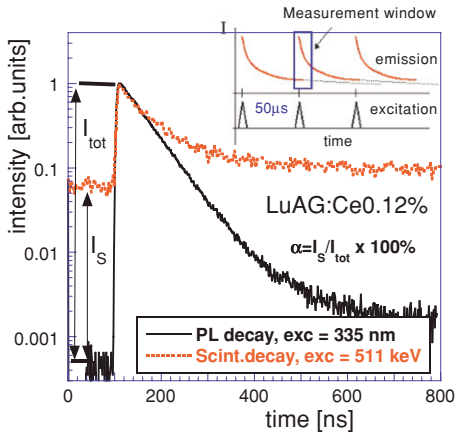

Figure 3. Normalized photoluminescence (PL) and scintillation decays of $Lu_3Al_5O_{12}$:Ce single crystal measured at 500 nm and in spectrally unresolved mode, respectively, under comparable experimental conditions at room temperature. The signal level before the rising edge of PL decay represents the true value of the background due to photo-detector noise. An increased level of signal before the rising edge of the scintillation decay is due to longer decay components, which are still surviving from preceding excitation events, see the sketch in the inset. A coefficient alpha is defined to quantitatively appreciate the contribution from such very slow decay processes.

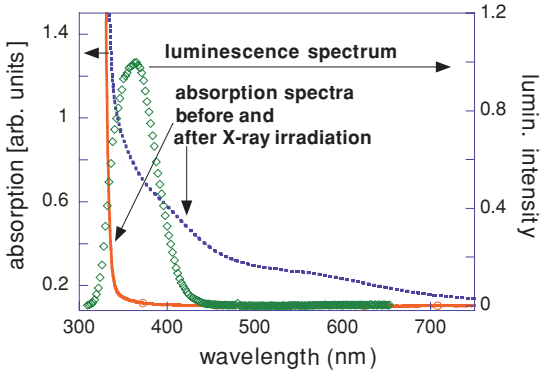

Figure 4. Absorption spectra of 2 cm thick $YAlO_3$:Ce single crystal before and after γ-ray irradiation (^{60}Co, 500 Gy dose) at room temperature. Overlap of the irradiation induced absorption with the luminescence spectrum of the material is demonstrated.

in figure 3. In practical evaluation of both phosphors and scintillators sometimes simple 1/e (cf equation (3)) or 1/10 decay times are provided, which are defined as the time when the light intensity decreases to 1/e or 1/10 of its initial intensity after a flash excitation or so-called mean decay time can be calculated [10] as well.

Spectral matching between the phosphor/scintillator emission band and the photodetector spectral sensitivity dependence is an obvious requirement and classical criteria were defined a time ago as that the near UV–blue emission is an optimum for a photomultiplier detector, while for a photodiode the green–red spectral region was considered the best. In the recent years an enormous development of semiconductor photodetectors has occurred and the latest generation of the back illuminated CCD from Hamamatsu announced for 2005 shows an enhanced sensitivity down to 200 nm.

Chemical stability concerns mainly the hygroscopicity of materials, which in some cases severely limits their long-time operation in the open air (NaI:Tl, CsI:Na, $LaBr_3$:Ce). Usual operating conditions, however, do not induce any kind of chemical reaction, which is currently a matter of concern in the development of the new generation of cathodoluminescent phosphors for field emission displays—successors of old CRT-based devices. In this case lower operating voltage and higher current densities require special technological consideration to prevent phosphor decomposition, especially in the case of (oxy)sulfides [27].

Radiation resistance of materials regards mainly the changes and performance instabilities due to the induced absorption resulting from material irradiation and colour centre creation. It is a matter of concern mainly in bulky scintillation elements, see e.g. [10]. In the case of the induced absorption overlap with the emission spectrum the re-absorption losses occur with resulting loss of the overall efficiency/light yield: an example is given in figure 4. While this parameter has been considered mainly in the research on scintillators for high-energy physics, it should be noted that it has importance also in some of the medical imaging techniques [13] and in the case of industrial flaw detection or synchrotron beam diagnostics applications as well.

Linearity of light response with incident x-ray dose and intensity required in phosphors differs considerably in its nature from the demand on the linearity of light response with incident x(γ)-ray photon energy in scintillators. While in the former case we are dealing mainly with the saturation or stability related issues, in the latter case the underlying physical phenomena are more intriguing. The fact that light yield value is energy dependent is partly due to abrupt changes of the attenuation coefficient around the K and L edges of the elements constituting the compound, but it also follows from the non-equal conversion efficiency of the photoelectric and Compton scattering effects, which becomes progressively more important with the increasing energy of incoming x(γ)-rays. As a result the energy resolution of a scintillator material is noticeably degraded with respect to the intrinsic limits based purely on statistical grounds [28]; for more information on this subject see [29, 30].

The very last parameter considered in the case of powder phosphors or other forms of scintillator materials used in screen applications—spatial resolution across the screen—is determined mostly by the geometry and morphology of the phosphor layer itself, namely its thickness, phosphor grain size and shape, void content, usage or nonusage of an optical binder, etc. Contradictory requirements come from the need for high spatial resolution (thin screen needed) and high x-ray stopping power (thick screen needed), which also applies in the case of single crystalline thin film/plate screens used for the high resolution 2D-imaging [31]. A thick powder screen also diminishes the amount of light available at the external photodetector due to multiple light scattering. The spatial resolution is currently characterized by the transfer function, which maps the incident x-ray image onto the output light image. The so-called point spread function (PSF) or modulation transfer function (MTF) is used for this purpose; for more information see [32]. A breakthrough in this parameter was realized by the preparation of microstructured scintillator layers in the form of thin (few μm diameter) and

long (up to 1–2 mm) ordered and densely packed needles of CsI-based scintillators coupled to position-sensitive detectors, which, due to their light guiding effect, can keep high spatial resolution even with the layer thickness exceeding 1 mm, i.e. high x-ray stopping power is realized as well [32–34].

2.2.2. Measurement methods. The methodology of radiation detection is collected in [4]. To quantify the characteristics and parameters described in section 2.2.1 a set of routine methods is usually used.

Overall efficiency of x-ray-to-light conversion is frequently measured in a relative manner, i.e. the studied material is compared with some 'standard' sample. Either an analogue of small size of phosphor screen is set and measured by an appropriate detector for a considered application, e.g. CCD in [18], or it is a routine measurement of radioluminescence spectra under defined x-ray excitation, see e.g. [8]. But in both cases care must be taken to perform the measurements in well-defined experimental conditions to get results for different materials–powders comparable in an absolute way. Namely, x-ray energy and powder layer thickness and its settling should be chosen in such a way to get complete x-ray absorption in all the materials measured. Registered light intensity can be noticeably influenced by the grain size, shape and surface treatment. Such measurements are comparatively easier for the bulky scintillators as exactly defined and all-polished samples of the same shape can be prepared, see e.g. [10] and figure 5(*a*). Truly absolute measurements of this parameter are extremely difficult and obviously 'sample-preparation dependent' and that is why the literature data in this respect vary considerably [6, 14, 23, 35]. It is obvious that even a relative measurement of radioluminescence spectra provides information about the emission positioning and its matching or nonmatching with the intended photodetector.

In the case of light yield measurement the pulsed x-ray source or (more often) γ-radiation lines from radioisotopes are used to excite the sample and measurement must be performed in a photon counting mode, i.e. with sufficiently low excitation rate to allow for a complete restoration of the detection chain after each registered event. The light flash generated per each x-ray pulse or per incoming γ-photon is converted in the photodetector into electrical current, which is integrated over a defined time gate at the output resistor with the help of a charge amplifier. The amplitude of the output pulse of the latter unit is then proportional to the incident light sum and is registered in a multichannel analyser. The measurement cycle is repeated many times to get a satisfactory signal-to-noise ratio. A very important condition for this measurement is that complete absorption of the incident x(γ) photons occurs in the sample to get a well-defined photopeak, the position of which is then decisive for the light yield determination, while its full width at half maximum (FWHM) determines the energy resolution [36]. As this measurement can be calibrated using the registration of the so-called single-photoelectron response [37], the position of the photopeak truly determines the number of photoelectrons generated in the photodetector. Using the quantum efficiency curve of the detector, it can be converted to the number of registered photons. However, this result is still different from the number of truly generated photons in the material due to geometrical losses in the light pass to the photodetector. Again, a large scatter of light yield values exists in the literature and often this measurement is used in a relative manner, i.e. with a kind of 'standard scintillator sample' for comparison with the studied material, see e.g. [5, 9–13, 30, 36–38].

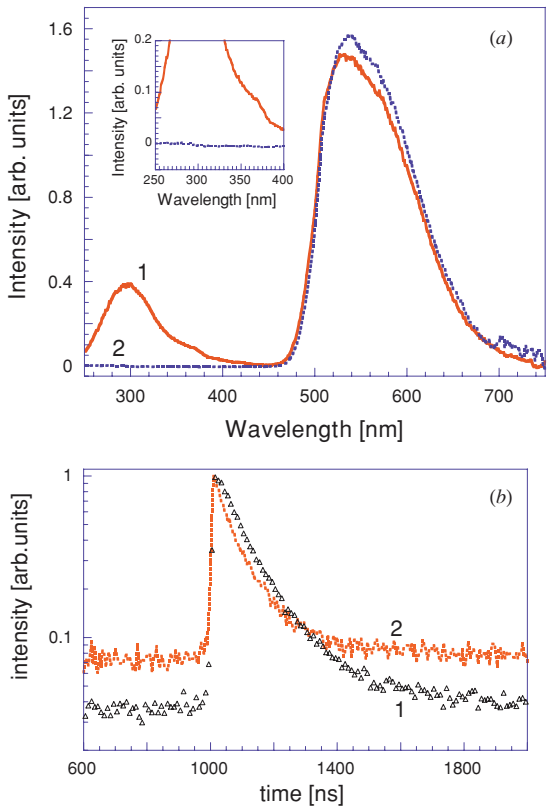

Figure 5. (*a*) Radioluminescence spectra (Mo cathode, 35 kV) of YAG:Ce single crystal (1) and ceramic (2) scintillators at room temperature. In the inset the enlargement of the 250–400 nm spectral region is provided to illustrate the complete absence of the 300 nm band in the ceramic. (*b*) Scintillation decay of the YAG:Ce single crystal (1) and ceramic (2) scintillators at room temperature. Spectrally unresolved excitation by 511 keV photons of ^{22}Na radioisotope. Approximation by the sum of exponentials considering also the instrumental response (see e.g. [10, 24, 25]) yields the decay time of 119 ns (1) and 85 ns (2) in the dominant decay component.

Measurements of scintillation response or afterglow in phosphors provide, together with the above measurements of material efficiency, the most important characteristics, which are carefully and systematically measured in a number of research and industrial laboratories due to their utmost significance in practical applications. Scintillation response (decay) is measured using the pulse x-ray (ps–ns pulses available, see [39, 40]), or γ-ray (radioisotopes employed) excitation and registration of luminescence decay is accomplished by the time-correlated single photon counting [41]. The measurement of decay curves and extraction of decay times (curves are usually approximated by the sum of exponential functions—equation (3)) are limited as for the shortest times by the instrumental response to the excitation pulse. Decay times down to about 100 ps can be extracted [39], while for the longest times (few tens of μs) the limiting factor arises due to the need of appropriately reduced excitation

frequency and the resulting consequence of worsening signal-to-noise ratio. Apart from an immediate fitting of the decay curve in the measurement window, the repetitive nature of the measurement gives the possibility of evaluating from the signal level before the rising edge of the scintillation response the amplitude of decay components, the mean time of which is comparable with the excitation frequency, i.e. giving an idea about the delayed recombination processes in the time scale tens to hundreds of μs, see figure 3 and [10]. It is worth noting that the occurrence of the delayed recombination processes due to charge carrier retrapping at shallow traps can usually be monitored by standard thermoluminescence (TSL) measurements and correlations between the very slow components in the scintillation decays (afterglow in phosphors) and the occurrence and amplitude of TSL glow curve peaks below room temperature were reported for several materials [26, 42, 43].

Measurement of afterglow in phosphors is accomplished by (even mechanical) cutoff of the steady-state x-ray excitation and subsequent registration of the luminescence decay on a time scale down to units–hundreds of ms [18, 23]. On this time scale direct sampling of the decay is technically accessible by a boxcar averaging detector (analogous signal from the photodetector), or using the multichannel scaling principle or gated photon counters if the photon counting mode is used in the photodetector.

Radiation resistance of the materials can be tested by measurement of the induced absorption in the case that bulky transparent optical elements can be obtained from the material. In this case the induced absorption IA is obtained as

$$\mathrm{IA}(\lambda) = 1/d \ln(T_{\mathrm{irr}}(\lambda)/T_0(\lambda)), \qquad (4)$$

where d is the thickness of the sample, and T_{irr} and T_0 are the transmittance of the sample after and before x-ray irradiation, respectively, see e.g. [10, 44]. More direct evaluation of (in)stability of material under a radiation load, applicable also to phosphors, is obtained by the measurement of the dependence of the overall conversion efficiency or light yield on the incident x(γ)-ray dose, see e.g. [45].

3. Materials

As was stated in the introduction, the need for x-ray-to-light converting materials appeared immediately after the initial observation of x-rays. The $CaWO_4$ and ZnS-based phosphor powders were introduced in practice very soon after and can be found in a limited number of applications up to the present day. In the late forties the first single crystal scintillators NaI:Tl and CsI:Tl appeared and have been widely used till today due to their low production cost and high overall efficiency. Finally, the latest class of materials—scintillation optical ceramics—became of use relatively recently when appropriate technology was developed to obtain competitive material properties mainly for materials where single crystals cannot be prepared or their production is extremely expensive.

3.1. Powders

An early survey of the activities in the field of x-ray phosphor development was given by Brixner [8]. $CaWO_4$ phosphor was dominantly used until the seventies, when new, more efficient materials based on Tb-doped oxysulfides (R_2O_2S, R = Y, La, Gd) appeared and their potential for x-ray detection was recognized [46]. Among them the Gd_2O_2S host showed the highest figure-of-merit due to elevated density and effective atomic number. Several different dopants were studied in this host, namely Tb, Eu, Pr, Nd and Dy, see e.g. [18, 47] for a survey. In practice the most important, Tb^{3+} (dominant emission peak at 540 nm) and Pr^{3+} (dominant emission peak at 490 nm) doping was distinguished. Codoping by Ce and by (Ce, F) was found to decrease the afterglow [18, 48]. These materials have been studied further in recent years for their spectroscopical characterization, performance limits [47, 49, 50] and new technological ways for their preparation [51, 52].

Other efficient phosphors are based on rare earth ion doped oxyhalides LnOX (Ln = Y, La, Gd; X = Cl, Br). First studies date back to the fifties [53], but the potential of these compounds, namely of Tb^{3+}- and Tm^{3+}-doped LaOBr, was fully recognized about 20 years later (for a review see [8]). Both phosphors show the dominant emission line in the blue spectral region at about 420 and 470 nm, respectively. The overall efficiency of Tb^{3+}-doped LaOBr approaches that of Gd_2O_2S:Tb [12]. Luminescence properties of Tb-doped GdOBr were reported recently [54].

Frequently reported materials are rare earth doped binary oxide Ln_2O_3 (Ln = Y, Gd, Lu) doped dominantly with Eu^{3+}. While Y_2O_3:Eu is a well-known red emitting phosphor [3] used in lighting and CRT applications, attention is paid to the other two compounds due to their elevated density and the possibility of preparing optical ceramics, see section 3.2. In the case of Gd_2O_3 host, attention has been paid in recent studies to codoping as a tool for efficiency enhancement or the possibility of finding HfO_2-mixed compounds of higher density [55–57]. The effects of the surface 'dead layer' and the grain size itself in a nanocrystalline powder were studied for the influence on the material luminescence shape and efficiency [58, 59]. Lu_2O_3 host offers exceptionally high density of about 9.4 g cm^{-3}, which, together with the $LuTaO_4$-based phosphors (9.75 g cm^{-3} [8]), is the densest phosphor available. Recent studies deal with the spectrocopic properties in the case of Eu^{3+} and Tb^{3+} doping [60, 61].

An interesting phosphor as regards its luminescence mechanism is Sr_2CeO_4: one of very few examples where emission is produced due to charge transfer (ligand-to-metal) luminescence of the Ce^{4+}-based complex. This compound was identified by the combinatorial approach from more than 25 000 species prepared by automated thin-film synthesis [62]. The broad emission band peaks at 485 nm and shows the decay time of about 51 μs and quantum efficiency $Q = 0.48$ at room temperature. Luminescence characteristics are determined by the spin-forbidden character of the oxygen–Ce^{4+} charge transfer transition. Different preparation methods and more detailed characterization were described in the literature, e.g. synthesis by the solid-state reaction [63], spray pyrolysis [64] and pulsed-laser deposition [65]. Recently, a sol–gel method using a polymer dispersing medium was described claiming to provide more homogeneous particle size of about 1 μm and uniform crotch-like morphology [66].

Phosphors containing hafnium are worth mentioning as they can constitute host materials of high density, but with

Table 1. A survey of characteristics of selected phosphor materials [6, 7, 12, 13, 18, 89].

Phosphor	Density (g cm^{-3})	Decay time (ns)	Efficiency η (%)	Emission maximum (nm)	Afterglow
ZnS:Ag	3.9	~1000	17–20	450	Very high
$CaWO_4$	6.1	6×10^3	5	420	Very low
Gd_2O_2S:Tb	7.3	6×10^5	13–16	540	Very low
Gd_2O_2S:Pr, Ce, F	7.3	4000	8–10	490	Very low
LaOBr:Tb	6.3	~10^6	19–20	425	Low
$YTaO_4$:Nb	7.5	~2000	11	410	Low
Lu_2O_3:Eu	9.4	~10^6	~8	611	Medium
$SrHfO_3$:Ce	7.7	40	2–4	390	Not reported

practically no background radioactivity resulting in higher background noise, which is inevitably present in the Lu-containing compounds due to the natural abundance of ^{176}Lu radioisotope. An interest appeared recently in the case of $SrHfO_3$ host, which was doped by Ce^{3+} or Tm^{3+} [67–69], to obtain an efficient phosphor emitting in the violet–blue spectral region. The effect of codoping was studied as well in relation to the occurrence of the unwanted Ce^{4+} oxidation stage [70]. Several compositions based on Ce-doped BaO, HfO_2, Y_2O_3 and Lu_2O_3 raw constituents were prepared by the solid state reaction and their luminescence properties were examined [71].

There are a number of other compounds studied in the light of the x-ray phosphor or field emission display (FED) phosphor applications in the recent literature. The material requirements are quite similar in both application fields, especially if lower energies of x-rays (below 20 keV) are considered. Compositions of AB_2O_4 (A = Sr, Zn, Ca; B = Ga, In, Y) doped mostly with Mn^{2+}, Cr^{3+}, Eu^{3+}, Tb^{3+}, Eu^{3+} or other rare earth ions can be mentioned, see e.g. [72, 73] and references therein. Ternary sulfides are also frequently researched due to their lower energy gap with respect to oxides and thus the possibility of getting higher overall conversion efficiency. Compositions such as AB_2S_4 (A = Ca, Sr, Ba; B = Ga, Y, Al) doped with Mn^{2+}, Ce^{3+} or Eu^{3+} are most frequent, see e.g. [74–76]. The orthosilicates Ln_2SiO_5 (Ln = Y, Lu) doped with Ce^{3+}, Tb^{3+} and Eu^{3+} have been reported as well [77, 78]. Finally, it is interesting to note quite numerous studies on powders of $Y_3Al_5O_{12}$ (YAG) doped mostly with Ce^{3+}, Tb^{3+} and Eu^{3+} ions (see e.g. [79–81]) where new or unconventional preparation technologies are employed. A survey of characteristics for selected materials is given in table 1.

3.2. Optical ceramics

These transparent or translucent materials are constituted by tight aggregating crystallite micro-grains, each randomly oriented with respect to their neighbours. They have been under development as an alternative to the single crystal materials to provide bulky optical elements in the case where single crystals cannot form or when ceramic materials show superior properties e.g. in the achievable concentration and homogeneity of the dopant. Their technology has greatly developed mainly within the last one to two decades, when, in the case of cubic material, the progress in technology allowed bulky elements visually indistinguishable from single crystals and in some parameters (doping profile) clearly superior, to be obtained. Among the developed materials it is mainly YAG:Nd and Y_2O_3:Nd which reached the highest degree of perfection and their primary application is in the field of solid state lasers [82, 83]. The size of the single crystal grains is of the order of a few tens of microns, interface thickness is reported to be about 1–2 nm only and the residual volume of pores to be about several ppm.

It is worth noting that the application demands are clearly higher in the case of scintillators than laser optical ceramics. In the latter case it is mainly the scattering loss due to pores (voids) and grain interfaces which can limit the material performance. Already achieved reduction of the pores' volume down to a few ppm and interface thickness to a few nm reported in [82, 83] is enough to make them fully comparable to their single crystal analogues. However, in the case of scintillators, even the point defects at the atomic scale can seriously limit the material performance due to the introduction of trapping levels in the material forbidden gap (see section 2). If we consider the grain size of the order of a few tens of μm and thickness of the interface layer 1–2 nm, then the expected concentration of the interface-related (trapping) states may easily reach several hundreds of ppm. Such concentration can noticeably influence the characteristics of the transport stage (figure 2) due to retrapping of the migrating carriers or even by the introduction of nonradiative traps, which can seriously degrade the scintillation response and/or overall efficiency parameters.

Development of such materials for the scintillator applications was triggered by the needs of computer tomography (CT) medical imaging [13] and the review of the results achieved mainly at the manufacturing and characterization of (Y, Gd)$_2O_2$:Eu, Gd_2O_2S:Pr, Ce, F and $Gd_3Ga_5O_{12}$:Cr, Ce ceramics was reported by Greskovich [84]; see also [48, 85–87] for more details about the particular materials. In the latter two materials codoping by Ce^{3+} is used to reduce the afterglow, which is accomplished by the capture of holes at Ce ions, $Ce^{3+} \rightarrow Ce^{4+}$ conversion and subsequent nonradiative recombination with migrating electrons and/or temporary Eu^{2+} centres, see also [18]. In further optimization of (Y, Gd)$_2O_2$:Eu [88] codoping by Pr^{3+} appeared as an efficient tool to reduce the ceramic's afterglow (by a similar mechanism to that of the Ce ions above) and the annealing in the controlled atmosphere can further diminish or passivate the trapping states in the forbidden gap related to the grain interfaces.

Among the new optical ceramics suggested for scintillator applications are namely the Eu^{3+}- or Tb^{3+}-doped Lu_2O_3 mentioned already in section 3.1. True optical ceramic Lu_2O_3:Eu samples were synthesized, their performance tested in comparison with CsI:Tl and a large area scintillation screen was prepared [89, 90]. While providing 60% of the emission

intensity of CsI:Tl, a better match to the CCD photodetector sensitivity was concluded. An afterglow noticeably distorted the exponential decay of Eu^{3+} at times above 6 ms and its mechanism was studied further in [91]. This compound was also prepared by a sol–gel and molten salt-route synthesis and characterized by luminescence methods [92, 93].

Recently, Ce-doped YAG optical ceramics became available from Baikowski, Japan Ltd, the production technology of which should be analogous to that of YAG:Nd described in [82]. YAG:Ce is a well-known scintillator [94] and in figures 5(*a*) and (*b*) the comparison is made between equally shaped samples (ø 15 × 1 mm) of an industrial standard quality single crystal YAG:Ce produced by CRYTUR, Ltd, Czech Republic and the aforementioned optical ceramics. Strongly different Ce concentration was present in both samples: while in the single crystal concentration of about 1000 ppm was measured, in the ceramic system concentration of about 5000 ppm was obtained. While the radioluminescence intensity in the dominant Ce^{3+}-related band round 550 nm is comparable in both samples (figure 5(*a*)), it is interesting to note a complete absence of the 300–350 nm band in the ceramic sample. This band is ascribed to a luminescence centre based on an antisite Y_{Al} defect [95] and its formation crucially depends on the preparation temperatures. In the liquid phase epitaxy thin film of YAG:Ce (growth temperature ∼1000 °C with respect to 1900–1950 °C in the case of the Czochralski grown single crystal) these defects and the 300–350 nm emission band are absent [96]. As the preparation temperatures of YAG-based optical ceramics are noticeably lower with respect to the single crystal, it can be concluded that the Y_{Al} antisite defects are absent in the former system. Normalized scintillation decays are given in figure 5(*b*). The ceramic material shows faster decay, the decay time of which is closer to the photoluminescence lifetime of the Ce^{3+} centre (about 60–65 ns). It can be explained by higher Ce concentration and the absence of the Y_{Al} antisite defects. However, it contains higher content of very slow scintillation components, which is reflected in lower amplitude-to-background ratio; see also figure 3 and [10, 24] for more details. The presence of such very slow decay components is usually related to the enhanced presence of the traps reflected in TSL measurements below RT and, indeed, in this case the ceramic system shows higher intensity of the TSL glow curve above approximately 190 K [97], which may point to the involvement of the traps related to the grain interfaces.

3.3. Microstructured materials

These materials were developed to meet the demand of increased x-ray stopping power, while keeping high spatial resolution on the imaging screens, see the end of section 2.2.1. In the case of a few scintillation materials, namely CsBr:Tl [98], CsI:Na [99] and CsI:Tl [100–102], it is possible to prepare them by vacuum evaporation in the form of long (up to 1–2 mm) and thin (several μm diameter) needles, which are densely packed and optically isolated (figure 6). Such a needle layer can be directly deposited on the photodetector and due to the light-guiding effect in the needles it preserves high spatial resolution with the increased layer thickness, which ensures higher x-ray stopping power. Also a theoretical model was developed to describe the conditions for such growth morphology [103]. While this concept has been used for a long time for CsI:Na in image intensifiers [104], where CsI:Na is on the inner side of the photocathode, i.e. in vacuum, it could not be used in the open atmosphere due to the extreme hygroscopicity of CsI:Na. Only the development of this growth morphology for much less hygroscopic CsI:Tl, and an availability of large area position-sensitive semiconductor detectors (CCD, a-Si:H panels), enabled the construction of a new generation of flat panel detectors, which provide a qualitative upgrade in many kinds of medical, industrial and scientific imaging; see [13, 32, 105] and the more detailed description in sections 4 and 5.

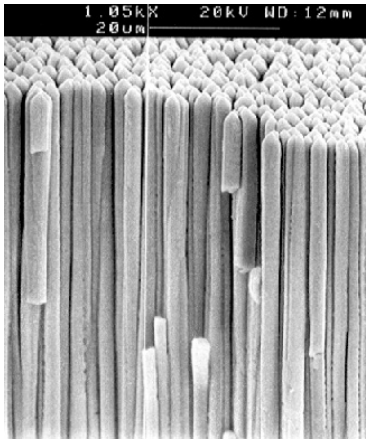

Figure 6. Vapour deposited column-shaped CsI:Tl scintillation crystals of very smooth structure. Diameter ∼3 μm, length >0.5 mm. Reprinted from [13] with permission (courtesy Philips Research Laboratories, Aachen).

3.4. Single crystals

The history of the true bulky single crystal scintillators began in the late forties with the introduction of NaI:Tl and CsI:Tl scintillators [20, 21] and from that time a number of similar material systems for this use have been reported; see [12] for a historical overview. Together with the above two materials $Bi_4Ge_3O_{12}$ (BGO) introduced by Weber and Monchamp in 1973 [106] also became a widespread scintillator and is often used as a 'standard scintillator' in comparison with newly developed materials. Within the last 15 years there has been considerable activity in this field triggered mainly by the need of high-energy physics and advanced imaging applications in science, medicine and industry. It has led to a considerable number of articles in the literature dealing mostly with the Ce^{3+}-doped materials, for a review see [107, 108], due to the fast decay time of the 5d–4f radiative transition of Ce^{3+} centre (typically 20–60 ns) and its high quantum efficiency (close to 1) at room temperature. A survey of practically important and/or intensively researched materials is given in table 2.

The interest in heavy, fast and efficient materials was focused mainly on the Lu-compounds and as a result new high figure-of-merit Lu_2SiO_5:Ce (LSO:Ce) and $(Lu_xY_{1-x})_2SiO_5$:Ce

Table 2. A survey of characteristics of selected single crystal scintillators [5, 13, 128, 136, 143].

Crystal	Density (g cm^{-3})	Light yield (photon MeV^{-1})	Dominant scintillation decay time (ns)	Emission maximum (nm)	$\Delta E/E$ at 662 keV (%)
CsI:Tl	4.51	66 000	800	550	6.6
NaI:Tl	3.67	41 000	230	410	5.6
$LaBr_3$:Ce	5.3	61 000	35	358	2.9
K_2LaI_5:Ce	4.4	55 000	24	420	4.5
BaF_2 (only cross luminescence)	4.88	1 500	0.6–0.8	180–220	7.7
$Bi_4Ge_3O_{12}$	7.1	8 600	300	480	9.0
$PbWO_4$	8.28	300	2–3	410	30–40
$CdWO_4$	7.9	20 000	5 000	495	6.8
$YAlO_3$:Ce	5.6	21 000	20–30	360	4.6
$LuAlO_3$:Ce	8.34	12 000	18	365	~15
$Y_3Al_5O_{12}$:Ce	4.56	24 000	90–120	550	7.3
$Lu_3Al_5O_{12}$:Ce	6.67	12 500	55	530	11
Gd_2SiO_5:Ce	6.7	8 000	60	420	7.8
Lu_2SiO_5:Ce	7.4	26 000	30	390	7.9

materials were studied, optimized and their production was industrialized afterwards [109–112]. Its lower performing structural analogue Gd_2SiO_5:Ce (GSO:Ce) [113] was also noticeably improved [114] and recently Zr-codoping was used to further increase its light yield and limit the Ce^{4+} occurrence [115]. In both cases large single crystals are commercially available from industrial producers, even if their production is expensive due to their very high melting point over 2000 °C, costly raw materials and demanding technology. Ce-doped lutetium pyrosilicate was recently announced as a new promising scintillator [116] within the silicate group, but only small samples have been prepared and studied so far.

Interest and research effort was paid by several groups to the development of the Lu-analogue of the well-known $YAlO_3$:Ce scintillator due to its higher density and x-ray stopping power [117–121]. The growth of $LuAlO_3$ single crystals is very difficult due to instability of the perovskite phase and an easy switch to the garnet ($Lu_3Al_5O_{12}$) one during the process [122]. Increased stability of the growth was found for the mixed (Y–Lu)AlO_3 systems, which were grown both by the Czochralski and Bridgman methods [123, 124], and finally this concept was chosen for the prototype industrial production [125].

$Lu_3Al_5O_{12}$ structure is stable and comparatively easier to grow. It has been studied for its scintillation performance as well [107, 126, 127]. $Lu_3Al_5O_{12}$:Ce crystals are already available from industrial production and the figure-of-merit of this material is comparable with GSO:Ce taking into account the x-ray stopping power, light yield and scintillation response parameters [127, 128]. Scintillation characteristics of this material were reported also in the form of thin single crystal films, typically of a few tens μm thickness, prepared by liquid phase epitaxy, which provides antisite defect-free material [96, 129]. Sc^{3+}-doped bulk crystals and thin films were also studied providing the intense, but slower emission round 280 nm, which is ascribed to the exciton trapped round Sc ions [130, 131].

It is worth mentioning that despite the attractiveness of Lu-based scintillators, their widespread applications might be limited by high cost of Lu_2O_3 and demanding technology, but also by the increased background due to the 2.59% natural abundance of ^{176}Lu radioactive isotope (half-life 3.78 × 10^{10} years), which results in about 300 background counts-per-second per each cm^3 of the material. Such a problem can be encountered also with other elements, for instance Rb (27.8% of ^{87}Rb, half-life 4.75 × 10^{10} years), K (0.0117% of ^{40}K, half-life 1.277 × 10^9 years) or to a lesser extent with La (0.0902% of ^{138}La, half-life 1.04 × 10^{11} years).

Recently, a new class of medium density halide scintillators appeared, which attracted attention mainly due to high light yield and very good energy resolution approaching the value of about 3% for 662 keV γ rays. Namely, Ce-doped binary compounds such as $LaCl_3$ and $LaBr_3$ were grown in single crystal form and their scintillation characteristics reported in [132, 133]. The advantage of the narrower band-gap and reasonable level of the energy transfer delaying processes due to self-trapped excitons (STE) [134], especially in the case of $LaBr_3$ host, further combined with favourable characteristics of the Ce^{3+} centre, resulted in an advanced figure-of-merit of these materials. The scintillation mechanism of these materials was further reviewed [135] including the role of V_K centres in the energy transfer processes, which is a key point in the transport stage characteristics of alkali halide scintillators. Furthermore, single crystals of ternary compounds K_2LaX_5:Ce were studied within the same collaboration [136] and K_2LaI_5:Ce appears to be an especially promising scintillator with density comparable to that of CsI, but much faster scintillation response governed by the 24 ns decay time of the Ce^{3+} centre itself. However, a relatively small Stokes shift of 0.17 eV may lead to bigger reabsorption losses in bulky optical elements. A major conclusion was drawn in [135, 136] that when the anion changes in the Cl→Br→I sequence, the lifetime of the STE shortens and the transfer speed from the STE and V_K centres towards Ce^{3+} tends to increase, which usually results in faster scintillation response. The drawback of these materials consists in enhanced hygroscopicity, which is comparable to or higher than that of NaI:Tl and imposes the need to operate these materials in hermetically sealed compartments. Furthermore, somewhat increased background counts due to the radioactive ^{138}La and especially ^{40}K isotopes are expected.

As an example of a Ce-free scintillator material, which has been intensively studied in the last decade due to its selection for high-energy physics detectors, the $PbWO_4$ single

crystal can be mentioned (for a review see [10]). Recently, several attempts were reported to increase its light yield by multiple doping and/or annealing to allow its use also in other applications, which take advantage of its high density, fast response and relatively cheap production. Double (Mo, A^{3+}), A = Y, La, doping was reported in [137, 138] completed later by more systematic studies also with codoping by Nb^{5+} [139, 140]. Numerous other doping combinations were reported [141] and the influence of annealing or melt non-stoichiometry (Czochralski-grown crystals) as well [142, 143]. Despite the fact that in the case of (Mo, Nb) double doping the overall efficiency measured by the comparison of radioluminescence spectra is comparable with BGO, there is a considerable number of very slow components in the scintillation decay [140] and the light yield in any of the samples studied and reported so far has not exceeded 10% of BGO.

3.5. Material optimization

The transport stage of scintillator conversion sketched in figure 2 was mentioned as a critical and badly predictable period, in which the material performance can be degraded by the defects and flaws arising in the manufacturing process. In all the materials the point intrinsic defects arise (cation and anion vacancies) as a result of general thermodynamic conditions and are further completed by extrinsic point (accidental impurities) or more extended (dislocations, grain and domain interfaces) ones. In many cases such defects introduce energy levels in the forbidden gap, which can be further involved in the capture of migrating charge carriers. In the process of material optimization it is the aim to diminish or inactivate such defects in the material structure to increase the material performance closer to its intrinsic limits. In the case of accidental impurities or extended structural defects the solution consists in the material purification and optimization of the technological process, respectively, to improve the material purity and structure. In the case of intrinsic defects an alternative solution is often used, namely to codope the material with another aliovalent ion(s) which do(es) not participate in the energy transfer and storage processes. Due to the mismatch between their charge state and that of the original substituted lattice ion the Coulombic equilibrium in the lattice is changed and it usually induces changes in the concentration of intrinsic point defects as well. An example can be given in the optimization of $PbWO_4$ scintillator by doping or codoping it by trivalent ions at the Pb^{2+} site [10, 137, 139], by codoping Zr^{4+} at the Y^{3+} site of $YAlO_3$:Ce scintillator [144] or by modification of the Gd_2O_2S:Tb^{3+} phosphor properties due to the doping by both divalent and tetravalent ions [145]. Other examples of this optimization strategy can be found in [55, 70]. In these cases TSL measurements serve as a sensitive probe, which can monitor the changing concentrations of trapping states involved in the energy transfer and capture processes.

In optical ceramics an alternative approach is used—the material is codoped by an ion of the same charge state as the lattice site (Ce^{3+} at the Gd^{3+} site), which compete for the hole capture with (unknown) intrinsic traps and later on serves as a nonradiative centre at which the delayed migrating electrons recombine with previously captured holes. This approach proved very useful in decreasing the afterglow of Tb^{3+}- or Pr^{3+}-doped Gd_2O_2S or Eu-doped (Y, Gd)$_2O_3$ materials [18, 84–88]. In these materials annealing was also mentioned as a useful tool to diminish active traps at the grain interfaces [88]. Such an approach is frequently used in phosphor preparation as well due to the elevated surface area of the powder, but often it is a proprietary technology condition, which is not fully disclosed in the literature.

Another frequent problem is the aggregation of the doped ions—emission centres in the process of material preparation due to elevated temperatures (single crystal growth from melt, high temperature sintering of powders, etc). In the aggregated areas, due to high doped ion concentration, concentration quenching appears and absorbed energy in these aggregates is guided to nonradiative traps (killing sites) and lost, which strongly diminishes the material efficiency. In this case, especially in the preparation of powder phosphors or ceramic materials, other modern methods are explored, which can diminish this problem and ensure the homogeneous distribution of the dopant ions even at their high concentrations. The sol–gel method is especially worth mentioning as numerous reports in the recent literature show its potential for the above purpose, e.g. [66, 79, 81, 92]. Sol–gel preparations have also been demonstrated to provide inorganic bulk glass elements doped with organic dye emission centres but further work is needed to enhance efficiency [146].

4. Detector design

A composition sketch of a scintillator detector has already been shown in figure 1. The available phosphor and scintillator materials were discussed in detail in section 3. Their geometrical form and morphology can vary depending on the purpose. In most of the imaging screen applications the phosphor powder is settled into a thin layer of a few tens of mm [8, 147, 148], sometimes glued together with a suitable optical binder. Single crystal plates or films of a few μm thickness are exploited as well in microtomography or high 2D-resolution applications [31, 149]. Microstructured (columnary-grown) CsI-based scintillators can be prepared in 1–2 mm thick layers with an area over 1000 cm^2 in medical radiography [105]. Bulky single crystal and optical ceramic elements with a thickness of a few mm to a few cm, further structured or not, are also in use in various fields. In some cases, combination of two or more materials is used in so-called phoswich detectors to resolve incoming α, β and/or x(γ) radiation [150–152].

An optical relay element is missing in some configurations, e.g. in flat imaging panels [105], where microstructured CsI:Tl is directly deposited over the large area matrix of a:Si–H photodiodes (figure 7), or in the cases when such a scintillator layer is directly deposited on a CCD or attached to a CMOS position-sensitive photodetector [153, 154]. In cases where the scintillator material must be distant from the photodetector and 2D spatial resolution is required, the fibre optical taper (fibre optical plate) is mostly used. In some cases the optical relay chain can be complex, especially when the optical amplification by image intensifiers [13, 104] is used. Light amplification (intensification) is usually necessary to efficiently couple a phosphor screen

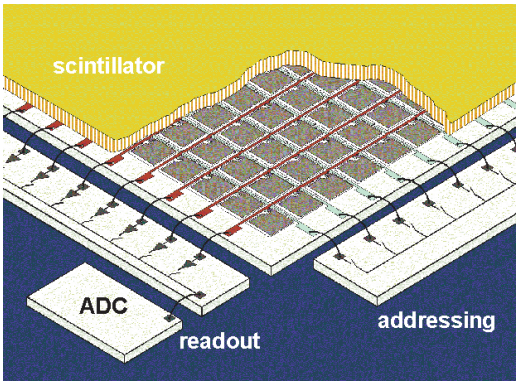

Figure 7. Schematic of a flat-panel detector. An array of amorphous-silicon diodes positioned on a glass plate is covered by a scintillator screen of columnar grown CsI:Tl. Addressing lines and readout lines are respectively coming from and going to chips at the edge of the plate. Reprinted from [13] with permission (courtesy Philips Research Laboratories Aachen).

of large area to a smaller area photodetector (demagnifying geometry) due to the fact that direct optical coupling is extremely inefficient (so-called quantum sink regime [155]) due to the low acceptance angle of the entrance lens. X-ray image intensifiers coupled with the CCD photodetectors offer an unmatched performance especially at low x-ray irradiation doses [156]. Fibre optical tapers can be used to interconnect all the elements in the detector or can be further combined with geometrical optics as well [157]. A systematic description of the optical relay and intensifier element configurations can be found in [32] and references therein.

Photomultipliers (PMT) are still the classic and the most sensitive photodetectors, in which in vacuum an electron ejected from the photocathode deposited on the inner side of the entrance window is accelerated and multiplied through a dynode chain and the gain reached may exceed 10^{10}. Position-sensitive photomultipliers are also readily available. However, photomultipliers are fragile, bulky, sensitive to magnetic field and of high manufacturing cost and are thus frequently being replaced by semiconductor detectors, if their sensitivity is sufficient. Recently, a hybrid PMT (HPMT) was developed [158]. It introduces a new tool, e.g. for scintillation photoelectron and light yield measurements [159]. The HPMT consists of an entrance window with the photocathode evaporated on its inner side and a small silicon diode placed opposite to the centre of the photocathode that acts as anode. Together with the focusing transversal electrodes all is sealed in a vacuum tube. The Si-diode detects the accelerated and electrostatically focused electrons liberated from the photocathode.

Let us consider the rich family of semiconductor photodetectors: apart from common photodiodes it is worth mentioning the fast development of avalanche photodiodes (APD), which combine the compactness of a semiconductor device and signal amplification (though noticeably less than in current photomultipliers). A large area APD tested in a scintillation detector has been reported recently [160, 161], and may become a serious competitor of PMT. Development is also occurring rapidly in the field of position-sensitive semiconductor detectors. Apart from widely spread CCD detectors, which revolutionized imaging technologies [32] due to remarkable linearity, low dark signal and read noise and high sensitivity performances, it is CMOS technology which can provide sensitive detectors with up to ten times lower power consumption and noticeably lower production cost [154]. The achievable dynamic range is also superior with respect to the state-of-the-art CCD detectors [157]. The CMOS figure-of-merit is degraded, however, by a lower speed and worse image quality with respect to CCD. Micromachined silicon detectors, in which an array of scintillator crystals is encapsulated in silicon wells with the photodiodes at the bottom, have also been considered for 2D-imaging with submillimetre resolution [162, 163]. Furthermore, large area silicon drift detectors were tested with CsI:Tl scintillator for achievable light yield, energy resolution and time response [164].

5. Applications

From a number of applications using x-rays across many fields of human activity, those from the area of medical imaging, general flaw detection, high resolution 2D-imaging and radio astronomy will be mentioned in more detail.

An in-depth overview of medical imaging principles, techniques and devices can be found in [13, 105, 165]. In medical imaging the applications can be divided into (i) static and (ii) dynamic imaging. General (chest, bone fractures, etc) and dental radiography together with mammography are the most frequently mentioned applications included in static imaging. Photographic film coupled to a Gd_2O_2S:Tb phosphor screen is still the workhorse configuration used all over the world, which is however gradually being replaced by modern flat panel detectors (figure 7) [166]. In general radiography a large image format is necessary (up to 43 $\times$ 43 cm^2 flat panels are commercially available) and pixel size is typically 100–150 μm square, and in dental imaging an image size of about 3 $\times$ 4 cm^2 is typically used with the pixel size about 20–40 μm square. In mammography special attention is paid to the detection of both very low contrast tumours in soft tissue and dense microcalcifications of a few hundred μm dimensions [167]. While higher x-ray energy between 60 and 120 keV is needed in general radiography, in the latter two application areas the usual values are between 20 and 30 keV. With respect to classical film-screen cassettes, the modern flat panel detectors offer at the same 2D resolution better sensitivity, higher dynamical range and the comfort of all-electronic image processing. In practice, such features of flat panel detectors result in improved image quality, easier and faster data handling, reduced running costs and also lower irradiation doses of patients.

In dynamical imaging it is namely fluoroscopy and computer tomography which use speedy data aquisition in real time and stringent requirements as for the afterglow are put on the phosphor/scintillator material. Fluoroscopy is an analogue of the above static imaging, where a progression-in-time of an image of a body part is to be followed, e.g. during interventional surgery, angiography examinations or other more general situations in which a distribution of a contrast agent in time is followed to detect a lesion. Typical frame rates (number of images taken per second (fps)) are between 15 and 30 fps and the above-mentioned flat panel technology was explored for this purpose as well [168].

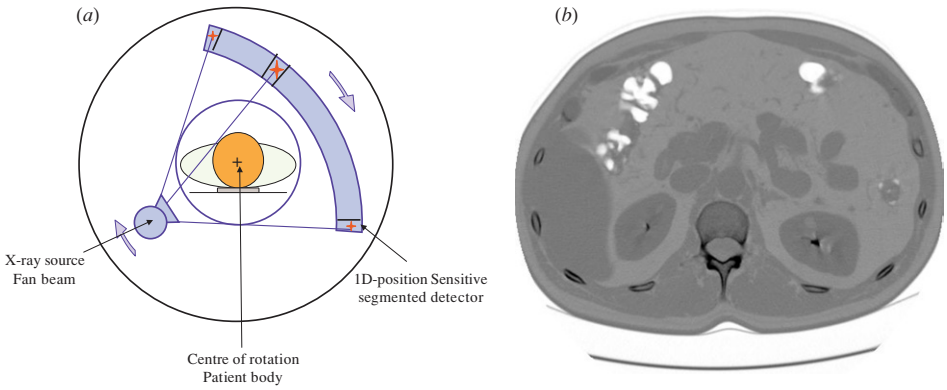

Figure 8. (*a*) Principle of computed tomography imaging. X-ray source providing a fan beam with an opposite 1D-position-sensitive segmented detector, mutually fixed on a common ground, which rotates around the patient body and many attenuation profiles are recorded within one 360° rotation. (*b*) CT scan picture—transversal slice of human body at the level of kidneys (courtesy of JR hospital, Sendai, Japan).

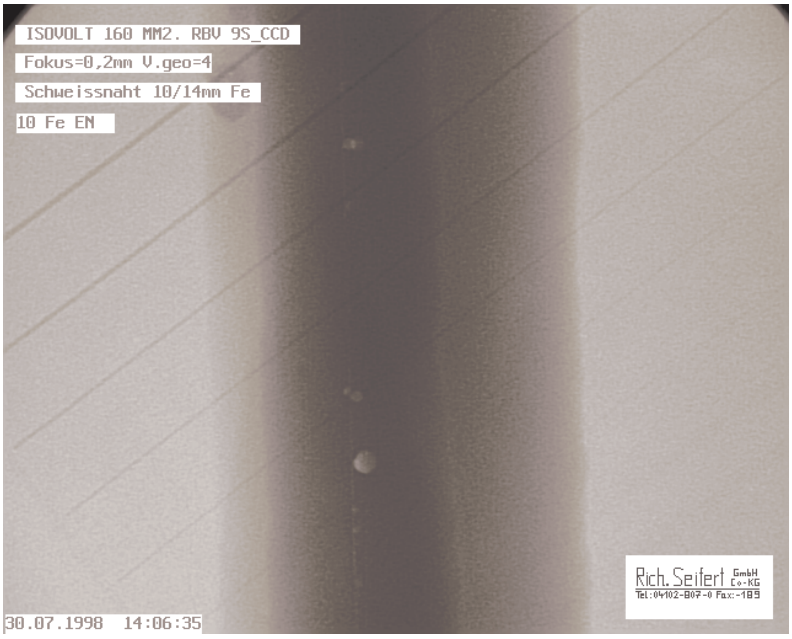

Figure 9. An x-ray image of a welding seam. Incompletely welded regions are revealed (thin vertical line in the middle) and bubbles in the welding are clearly seen as well. Overlayed inclined wires of decreasing diameter serve to monitor sufficient resolution and contrast of the image (courtesy of Seifert GmbH, Germany).

Computer tomography (CT) scanning has become a widely used technique to obtain transversal images of human body, the principle of which is shown in figure 8(*a*). An x-ray fan beam with a 1D-position-sensitive detector on a fixed construction rotates around the patient body in the centre with a typical frequency of 0.5–1 Hz and a large number of attenuation profiles is registered during one 360° rotation. From these data the cross-sectional images of the body are reconstructed (figure 8(*b*)). Applying simultaneously the slow gradual movement of the patient through the CT machine (so-called multi-slice spiral scan mode) even volume 3D-reconstruction images can be obtained. X-ray energies up to 140 keV are applied, which led to the need to apply dense ceramic materials with suppressed afterglow (see section 3.2).

Revealing hidden macroscopical flaws of materials is a long-term issue for non-destructive examination and among them particularly useful are those based on the registration of attenuation profiles of penetrating x-ray radiation. Energies of x-rays vary extremely, as for tiny non-metallic objects even soft x-ray sources are sufficient, while energies up to 450 keV are applied at the industrial flaw detection stations to check thick steel plates or welding of large diameter iron tubes, see also [169]. An image of a welding seam is shown in figure 9. It is interesting to note the overlayed wires of different diameters, the visibility of which ensures that sufficient contrast and resolution in the image is achieved.

In contrast to large-scale flaw detection stations in automotive and heavy industry there is a need to check the inner state and shaping of tiny objects where the resolution needed is of the order of a few μm or even less. Etched patterns and contact relief on wafers in the semiconductor industry or tiny biological objects can serve as an example. To achieve even submicron 2D resolution, the projection of an x-ray image created at a thin scintillator plate or film with

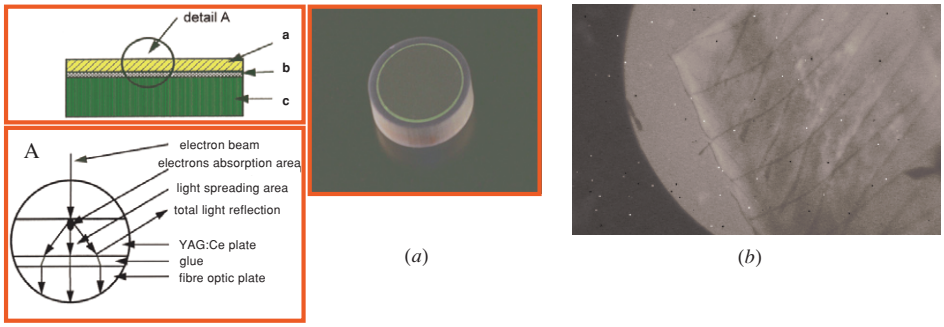

Figure 10. (*a*) A sketch of a high 2D-resolution x-ray or electron beam sensor head and the thickness-limited lateral resolution is given. A photograph of the sensor head is displayed as well. (*b*) A picture of the side of a dried aquarium fish with a clearly distinguished rib cage, 10–20 μm diameter (courtesy of CRYTUR, Turnov, Czech Republic).

the help of focusing geometrical optics can be used [31], but only soft x-ray or low energy electron beams can be used due to the thickness-limited stopping power of the scintillator. If resolution of several μm is enough, a compact arrangement can be used, which is sketched in figure 10(*a*)—about 5 μm thick YAG:Ce scintillator plate is glued onto a fibre optical plate and attached to a CCD sensor. Such a scintillation detector was used to x-ray a dried aquarium fish (figure 10(*b*)) and well-resolved rib cage of a thickness of about 10–20 μm can be observed illustrating the enhanced contrast capability of such a detector [170]. Such sensors can be easily used also in an industrial environment and/or in portable devices due to their compact and robust construction.

The last mentioned field in which scintillator detectors are used is radio (x-ray) astronomy. The first detection of x-ray emission from an extra-solar object was reported in 1962 [171] and from that time monitoring radiation in this energy window became one of the drivers of modern astronomy. The most important results obtained so far came from observations in the 'soft' x-ray band with photon energies between 0.1 keV and several keV and using the direct (i.e. non-scintillation) detection, the satellites Chandra and XMM-Newton can be mentioned as the most advanced missions [172, 173]. The hard x-ray energy range (~20–600 keV) has been explored comparatively less so far as x-rays are more difficult to focus and available scintillation detectors offer less advantageous spatial and energy resolution. NaI:Tl-based scintillation detectors were repeatedly used in recent satellite missions [174, 175]. A phoswich detector based on GSO:Ce and BGO was developed for Astro-E satellite recently [114]. Another mission considered for the future is the 'black hole finder probe', a large field of view, hard x-ray telescope. As one possible choice for the detectors the new scintillators $LaBr_3$:Ce or $LaCl_3$:Ce are under study due to their unique energy resolution capability [176]. A crucial condition for all scintillation materials to be used in such applications is an extremely low spontaneous background coming from radioactive isotope contamination due to the very low level of registered signals.

6. Conclusions

The all-the-time increasing number of applications of x-rays across many fields of human activity has stimulated the research into phosphor and scintillation material over the past 110 years. Its further acceleration over the last 10–20 years was induced by new demanding applications in the field of medical, industrial and scientific imaging and further development and exploitation of powerful x-ray sources such as e.g. synchrotron radiation. Thus intense research and development continues to look for new phosphor and scintillation materials or the optimization of the current ones taking advantage of new technological methods for their preparation. Understanding the underlying physical mechanisms of energy transfer and storage and the role of particular material defects in them is of crucial importance for bringing the materials performance close to the intrinsic limits. Other progress in the realization of the ideal detector design concerns the rapid development of the field of semiconductor photodetectors, which are an indispensable part of scintillation detectors.

Acknowledgments

The author acknowledges with sincere thanks C W E van Eijk and H Wieczorek for providing materials and discussion related to figures 6, 7, 8(*a*), H Sugawara for figure 8(*b*), Z Porkert for figure 9 and K Blazek for figure 10. Thanks are due to E Jurkova and N Mackova for their help in the literature search and J A Mares for useful discussions. Finally, the great help of D J S Birch in the final revision of the manuscript is deeply appreciated. Financial support of Czech Institutional Research Plan no AV0Z10100521, GA AV A1010305 and GA CR 202/05/2471 projects is also gratefully acknowledged.

References

[1] Röntgen W C 1895 Ueber eine neue Art von Strahlen *Sitz. Ber. Phys. Med. Ges. Wuerzb.* **9** 132–41 See also http://www.e-radiography.net/history/general.htm
Rontgen W C 1896 On a new kind of rays *Science* **3** 227–31
[2] Ozawa L and Itoh M 2003 Cathode ray tube phosphors *Chem. Rev.* **103** 3835–55
[3] Blasse G and Grabmaier B C 1994 *Luminescent Materials* (Berlin: Springer)
[4] Knoll G F 2000 *Radiation Detection and Measurement* (New York: Wiley)
[5] Rodnyi P A 1997 *Physical Processes in Inorganic Scintillators* (New York: CRC Press)
[6] Shionoya S and Yen W M 1998 *Phosphor Handbook* (New York: CRC Press)
[7] Yen W M and Weber M J 2004 *Inorganic Phosphors: Compositions, Preparation and Optical Properties* (New York: CRC Press)

[8] Brixner L H 1987 New x-ray phosphors *Mater. Chem. Phys.* **16** 253–81

[9] Ishii M and Kobayashi M 1992 Single crystals for radiation detectors *Prog. Cryst. Growth Charact.* **23** 245–311

[10] Nikl M 2000 Wide band gap scintillation materials. Progress in the technology and material understanding *Phys. Status Solidi* a **178** 595–620

[11] Wojtowicz A J 2002 Rare-earth-activated wide bandgap materials for scintillators *Nucl. Instrum. Methods Phys. Res.* A **486** 201–7

[12] Weber M J 2002 Inorganic scintillators: today and tomorrow *J. Lumin.* **100** 35–45

[13] van Eijk C W E 2002 Inorganic scintillators in medical imaging *Phys. Med. Biol.* **47** R85–106

[14] Robbins D J 1980 On predicting the maximum efficiency of phosphor systems excited by ionizing-radiation *J. Electrochem. Soc.* **127** 2694–702

[15] Lempicki A, Wojtowicz A J and Berman E 1993 Fundamental limits of scintillator performance *Nucl. Instrum. Methods Phys. Res.* A **333** 304–11

[16] Rodnyi P A, Dorenbos P and vanEijk C W E 1995 Energy loss in inorganic scintillators *Phys. Status Solidi* b **187** 15–29

[17] Vasil'ev A N 1996 Polarization approximation for electron cascade in insulators after high-energy excitation *Nucl. Instrum. Methods Phys. Res.* B **107** 165–71

[18] Shepherd J A, Gruner S M, Tate M W and Tecotzky M 1997 Study of afterglow in x-ray phosphors for use on fast-framing charge-coupled device detectors *Opt. Eng.* **36** 3212–22

[19] Kubota S, Ruan J, Itoh M, Hashimoto S and Sakuragi S 1990 A new type of luminescence mechanism in large band-gap insulators: proposal for fast scintillation materials *Nucl. Instrum. Methods Phys. Res.* A **289** 253–60

[20] Editors notes 1950 Properties of scintillation materials *Nucleonics* **6** 70–3

[21] VanSciver W and Hofstadter R 1951 Scintillations in thallium-activated CaI_2 and CsI *Phys. Rev.* **84** 1062–3

[22] Wilkinson J, Ucer K B and Williams R T 2004 Picosecond excitonic luminescence in ZnO and other wide-gap semiconductors *Radiat. Meas.* **38** 501–5

[23] Moy J P, Koch A and Nielsen M B 1993 Conversion efficiency and time response of phosphors for fast x-ray imaging with synchrotron radiation *Nucl. Instrum. Methods Phys. Res.* A **326** 581–6

[24] Nikl M 2005 Energy transfer phenomena in the luminescence of wide band-gap scintillators *Phys. Status Solidi* a **202** 201–6

[25] Nikl M, Nitsch K, Polak K, Mihokova E, Dafinei I, Auffray E, Lecoq P, Reiche P and Uecker R 1996 Slow components in the photoluminescence and scintillation decays of $PbWO_4$ single crystals *Phys. Status Solidi* b **195** 311–23

[26] Nikl M, Solovieva N, Pejchal J, Shim J B, Yoshikawa A, Fukuda T, Vedda A, Martini M and Yoon D H 2004 Very fast $Yb_xY_{1-x}AlO_3$ single crystal scintillators *Appl. Phys. Lett.* **84** 882–4

[27] Holloway P H, Trottier T A, Sebastian J, Jones S, Zhang X-M, Bang J-S, Abrams B, Thomes W J and Kim T J 2000 Degradation of field emission display phosphors *J. Appl. Phys.* **88** 483–8

[28] Valentine J D and Rooney B D 1994 Design of a Compton spectrometer experiment for studying scintillator non-linearity and intrinsic energy resolution *Nucl. Instrum. Methods Phys. Res.* A **353** 37–40

[29] Dorenbos P, de Haas J P M and vanEijk C W E 1995 Non-proportionality in the scintillation response and the energy resolution obtainable with scintillation crystals *IEEE Trans. Nucl. Sci.* **42** 2190–202

[30] Moszynsky M 2003 Inorganic scintillation detectors in γ-ray spectrometry *Nucl. Instrum. Methods Phys. Res.* A **505** 101–10

[31] Koch A, Raven C, Spanne P and Snigirev A 1998 X-ray imaging with submicrometer resolution employing transparent luminescent screens *J. Opt. Soc. Am.* A **15** 1940–51

[32] Gruner S M, Tate M W and Eikenberry E F 2002 Charge-coupled device area x-ray detectors *Rev. Sci. Instrum.* **73** 2815–42

[33] Cho H S, Hong W S, Perez-Mendez V, Kadyk J, Palaio N and Vujic J 1998 A columnar cesium iodide (CsI) drift plane layer for gas avalanche microdetectors *IEEE Trans. Nucl. Sci.* **45** 275–9

[34] Stevels A L N and Schrama-de Pauw A D M 1974 Vapour-deposited CsI:Na layers: I. Morphologic and crystallographic properties *Philips Res. Rep.* **29** 340–52
Stevels A L N and Schrama-dePauw A D M 1974 Vapour-deposited CsI:Na layers: II. Screens for application in x-ray imaging devices *Philips Res. Rep.* **29** 353–62

[35] Chappell J H and Murray S S 1984 Relative efficiencies and physical characteristics for a selected group of x-ray phosphors *Nucl. Instrum. Methods Phys. Res.* A **221** 159–67

[36] Moszynski M, Kapusta M, Wolski D, Szawlowski M and Klamra W 1998 Energy resolution of scintillation detectors readout with large area avalanche photodiodes and photomultipliers *IEEE Trans. Nucl. Sci.* **45** 472–7

[37] Moszynski M, Kapusta M, Mayhugh M, Wolski D and Flyckt S O 1997 Absolute light output of scintillators *IEEE Trans. Nucl. Sci.* **44** 1052–61

[38] Mares J A, Nikl M, Beitlerova A, D'Ambrosio C, de Notaristefani F, Blazek K, Maly P and Nejezchleb K 2003 Scintillation photoelectron $N_{phels}(E)$ and light $LY(E)$ yields of YAP:Ce and YAG:Ce crystals *Opt. Mater.* **24** 281–4

[39] Moses W W, Derenzo S E, Weber M J, Blankespoor S C, Ho M H and West A C 1995 Scintillator characterization using the LBL pulsed x-ray facility *Radiat. Meas.* **24** 337–41

[40] Nikl M, Mares J A, Solovieva N, Hybler J, Voloshinovskii A, Nejezchleb K and Blazek K 2004 Energy transfer to the Ce^{3+} centers in $Lu_3Al_5O_{12}$:Ce scintillator. *Phys. Status Solidi* a **201** R41–4

[41] Bollinger L M and Thomas G E 1961 Measurement of the time dependence of scintillation intensity by a delayed-coincidence method *Rev. Sci. Instrum.* **32** 1044–50

[42] Nikl M, Bohacek P, Mihokova E, Vedda A, Martini M, Pazzi G P, Fabeni P, Kobayashi M and Usuki Y 2002 Enhanced efficiency of doubly doped $PbWO_4$ scintillator *Radiat. Eff. Defects Solids* **157** 937–41

[43] Zych E, Brecher C and Glodo J 2000 Kinetics of cerium emission in a YAG:Ce single crystal: the role of traps *J. Phys.: Condens. Matter* **12** 1947–58

[44] Nikl M *et al* 1997 Radiation induced formation of color centres in $PbWO_4$ single crystals *J. Appl. Phys.* **82** 5758–62

[45] Tremsin A S, Pearson J F, Nichols A O, Pwens A, Brunton A A and Fraser G W 2001 X-ray-induced radiation damage in CsI, Gadox, Y_2O_2S and Y_2O_3 thin films *Nucl. Instrum. Methods Phys. Res.* A **459** 543–51

[46] Wickersheim K A, Alves R V and Buchanan R A 1970 Rare earth oxysulfide x-ray phosphors *IEEE Trans. Nucl. Sci.* **17** 57–60

[47] Creasey J P and Tyrrell G C 2000 Time-resolved photoluminescence and x-ray luminescence studies on rare-earth oxysulfide phosphors *Proc. SPIE—Int. Soc. Opt. Eng.* **3942** 114–21

[48] Yamada H, Suzuki A, Uchida Y, Yoshida M and Yamamoto H 1989 A scintillator Gd_2O_2S:Pr,Ce,F for x-ray computed tomography *J. Electrochem. Soc.* **136** 2713–6

[49] Cavouras D, Kandarakis I, Nomicos C D, Bakas A and Panayiotakis G S 2000 Measurement of the $(Gd,La)_2O_2S$:Tb phosphor efficiency for x-ray imaging applications *Radiat. Meas.* **32** 5–13

[50] Morlotti R, Nikl M, Piazza M and Boragno C 1997 Intrinsic conversion efficiency of x-rays to light in Gd_2O_2S:Tb powder phosphors *J. Lumin.* **72–74** 772–4

[51] Popovici E-J, Muresan L, Hristea-Simoc A, Indrea E, Vasilescu M, Nazarov M and Jeon D Y 2004 Synthesis and characterization of rare earth oxysulphide phosphors: I. Studies on the preparation of Gd_2O_2S:Tb phosphor by the flux method *Opt. Mater.* **27** 559–65

[52] Bang J, Abboudi M, Abrams B and Holloway P H 2004 Combustion synthesis of Eu-, Tb- and Tm-doped Ln_2O_2S (Ln = Y, La, Gd) phosphors *J. Lumin.* **106** 177–85

[53] Swindells F E 1954 Lanthanum oxychloride phosphors *J. Electrochem. Soc.* **101** 415–8

[54] Park J K, Kim C H, Han C-H, Park H D and Choi S Y 2003 Luminescence properties of GdOBr:Tb green phosphors *Electrochem. Solid-State Lett.* **6** H13–5

[55] Yi S, Bae J S, Shim K S, Jeong J H, Park J-C and Holloway P H 2004 Enhanced luminescence of Gd_2O_3:Eu^{3+} thin-film phosphors by Li doping *Appl. Phys. Lett.* **84** 353–5

[56] Seo Y S, Sohn K-S, Park H D and Lee S 2002 Optimization of Gd_2O_3-based red phosphors using combinatorial chemistry method *J. Electrochem. Soc.* **149** H12–8

[57] Chen J, Shi Y, Feng T and Shi J 2005 Synthesis of Eu^{3+}-doped Gd_2O_3–HfO_2 nanopowder for radiation detection *J. Alloys Compounds* **391** 181–4

[58] Ledoux G, Mercier B, Louis C, Dujarding C, Tillement O and Perriat P 2004 Synthesis and optical characterization of Gd_2O_3:Eu^{3+} nanocrystals: surface states and VUV excitation *Radiat. Meas.* **38** 763–6

[59] Mercier B, Dujardin C, Ledoux G, Louis C, Tillement O and Perriat P 2004 Observation of the gap blueshift on Gd_2O_3:Eu^{3+} nanoparticles *J. Appl. Phys.* **96** 650–3

[60] Zych E, Derec P J, Strek W, Meijerink A, Mielcarek W and Domagala K 2001 Preparation, x-ray analysis and spectroscopic investigation of nanosctructured Lu_2O_3:Tb *J. Alloys Compounds* **323–324** 8–12

[61] Zych E, Hreniak D and Strek W 2002 Spectroscopy of Eu-doped Lu_2O_3-based x-ray phosphor *J. Alloys Compounds* **341** 385–90

[62] Danielson E, Devenney M, Giaquinta D M, Golden J H, Haushalter R C, McFarland E W, Poojary D M, Reaves C M, Weinberg W H and Wu X D 1998 A rare-earth phosphor containing one-dimensional chains identified through combinatorial methods *Science* **279** 837–9

[63] van Pieterson L, Soverna S and Meijerink A 2000 On the nature of the luminescence of Sr_2CeO_4 *J. Electrochem. Soc.* **147** 4688–91

[64] Kang M-J and Choi S-Y 2002 Preparation of Sr_2CeO_4 blue phosphor by ultrasonic spray pyrolysis: effect of NH_4NO_3 addition *J. Mater. Sci.* **37** 2721–9

[65] Lee Y E, Norton D P, Budai J D, Rack P D and Potter M D 2000 Photo- and cathodoluminescence characteristics of blue-light-emitting epitaxial Sr_2CeO_4 thin-film phosphors *Appl. Phys. Lett.* **77** 678–80

[66] Chen S-J, Chen X-T, Yu Z, Hong J-M, Xue Z and You X-Z 2004 Preparation and characterization of fine Sr_2CeO_4 blue phosphor powders *Solid State Commun.* **130** 281–5

[67] Yamamoto H, Mikami M, Shimomura Y and Oguri Y 2000 Host-to-activator energy transfer in a new blue-emitting phosphor $SrHfO_3$:Tm^{3+} *J. Lumin.* **87–89** 1079–82

[68] Villanueva-Ibannez M, Le Luyer C, Parola S, Dujardin C and Mugnier J 2005 Influence of Sr/Hf ratio and annealing treatment on structural and scintillating properties of sol–gel Ce^{3+}-doped strontium hafnate powders *Opt. Mater.* **27** 1541–6

[69] Arai N, Kim T W, Kubota H, Matsumoto Y and Koinuma H 2002 Combinatorial fabrication and cathodoluminescence properties of composition spread $MHfO_3$:Tm^{3+} (M = Ca, Sr, Ba) films *Appl. Surf. Sci.* **197–198** 402–5

[70] Loureiro S M, Gao Y and Venkataramani V 2005 Stability of Ce(III) activator and codopant effect in $MHfO_3$ (M = Ba, Sr) scintillators by XANES *J. Am. Ceram. Soc.* **88** 219–21

[71] Borisevich A, Korzhik M and Lecoq P 2003 Luminescence of Ce doped oxygen crystalline compounds based on Hf and Ba *Nucl. Instrum. Methods Phys. Res.* A **497** 206–9

[72] Xu Z, Li Y, Liu Z and Wang D 2005 UV and X-ray excited luminescence of Tb^{3+}-doped $ZnGa_2O_4$ phosphors *J.Alloys Compounds* **391** 202–5

[73] Zhou L, Shi J and Gong M 2005 Red phosphor SrY_2O_4:Eu^{3+} synthesized by the sol–gel method *J. Lumin.* **113** 285–90

[74] Nakanishi Y, Nakajima H, Uekura N, Kominami H, Kottaisamy M and Hatanaka Y 2002 Influence of preparation conditions on the structural and luminescent properties of blue-emitting $SrGa_2S_4$:Ce thin film phosphors *J. Electrochem. Soc.* **149** H165–8

[75] Do Y R 2000 Cathodoluminescence properties of SrY_2S_4:Eu phosphor for application in field emission display *J. Electrochem. Soc.* **147** 1597–600

[76] Chartier C, Barthou C, Benalloul P, Chenot S and Frigerio J M 2003 Structural and luminescent properties of green emitting $SrGa_2S_4$:Eu thin films prepared by RF-sputtering *J. Cryst. Growth* **256** 305–16

[77] Han X M, Lin J, Fu J, Xing R B, Yu M, Zhou Y H and Pang M L 2004 Fabrication, patterning and luminescence properties of X_2–Y_2SiO_5:A (A = Eu^{3+}, Tb^{3+}, Ce^{3+}) phosphor films via sol–gel soft lithography *Solid State Sci.* **6** 349–55

[78] Huang H and Yan B 2005 Luminescence of nanophosphors Lu_2SiO_5 doped with different concentration of Tb^{3+} by *in situ* composition of hybrid precursors *Mater. Sci. Eng.* B **117** 261–4

[79] Choe J Y, Ravichandran D, Nlomquist S M, Kirchner K W, Forsythe E W and Morton D C 2001 Cathodoluminescence study of novel sol–gel derived $Y_{3-x}Al_5O_{12}$:Tb_x phosphors *J. Lumin.* **93** 119–28

[80] Lia X, Liu H, Wang J, Cui H and Han F 2004 YAG:Ce nano-sized phosphor particles prepared by a solvothermal method *Mater. Res. Bull.* **39** 1923–30

[81] Xia G, Zhou S, Zhang and Xu J 2005 Structural and optical properties of YAG:Ce^{3+} phosphors by sol-gel combustion method *J. Cryst. Growth* **279** 357–62

[82] Lu J, Ueda K, Yagi H, Yanagitani T, Akiyama Y and Kaminskii A A 2002 Neodymium doped yttrium aluminum garnet $Y_3Al_5O_{12}$ nanocrystalline ceramics—a new generation of solid state laser and optical materials *J. Alloys Compounds* **341** 220–5

[83] Lupei V, Lupei A and Ikesue A 2004 Single crystal and transparent ceramic Nd-doped oxide laser materials: a comparative spectroscopic investigation *J. Alloys Compounds* **380** 61–70

[84] Greskovich C and Duclos S 1997 Ceramic scintillators *Ann. Rev. Mater. Sci.* **27** 69–88

[85] Grabmaier B C and Rossner W 1993 New scintillators for x-ray computed tomography *Nucl. Tracks Radiat. Meas.* **21** 43–5

[86] Rossner W, Ostertag M and Jermann F 1999 Properties and applications of gadolinium oxysulfide based ceramic scintillators *Electrochem. Soc. Proc.* **98–24** 187–94

[87] Hupke R and Doubrava C 1999 The new UFC-detector for CT-imaging *Physica Medica* **XV** 315–8

[88] Duclos S J, Greskovich C D, Lyons R J, Vartuli J S, Hoffman D M, Riedner R J and Lynch M J 2003 Development of the HiLightTM scintillator for computed tomography medical imaging *Nucl. Instrum. Methods Phys. Res.* A **505** 68–71

[89] Lempicki A, Brecher C, Szupryczynski P, Lingertat H, Nagarkar V V, Tipnis S V and Miller S R 2002 A new lutetia-based ceramic scintillator for x-ray imaging *Nucl. Instrum. Methods Phys. Res.* A **488** 579–90

[90] Nagarkar V V, Miller S R, Tipnis S V, Lempicki A, Brecher A and Lingertat H 2004 A new large area scintillator screen for x-ray imaging *Nucl. Instrum. Methods Phys. Res.* B **213** 250–4

[91] Brecher C, Bartram R H and Lempicki A 2004 Hole traps in Lu_2O_3:Eu ceramic scintillators: I. Persistent afterglow *J. Lumin.* **106** 159–68

[92] García-Murillo A, Le Luyer C, Dujardin C, Martin T, Garapon C, Pédrini C and Mugnier J 2002 Elaboration and scintillation properties of Eu^{3+}-doped Gd_2O_3 and Lu_2O_3 sol–gel films *Nucl. Instrum. Methods Phys. Res.* A **486** 181–5

[93] Trojan-Piegza J and Zych E 2004 Preparation of nanocrystalline Lu_2O_3:Eu phosphor via a molten salts route *J. Alloys Compounds* **380** 118–22

[94] Moszynski M, Ludziejewski T, Wolski D, Klamra W and Norlin L O 1994 Properties of the YAG:Ce scintillator *Nucl. Instrum. Methods Phys. Res.* A **345** 461–7

[95] Volzhenskaya L G, Zorenko YuV, Patsagan N I and Pashkovsky M V 1987 Luminescent properties of $Y_3Al_5O_{12}$ monocrystalline compounds produced from melt and solution-melt *Opt. Spectra* **63** 135–40 (in Russian)

[96] Zorenko Yu, Gorbenko V, Konstankevych I, Voloshinovskii A, Stryganyuk G, Mikhailin V, Kolobanov V and Spassky D 2005 Single-crystalline films of Ce-doped YAG and LuAG phosphors: advantages over bulk crystals analogues *J. Lumin.* **114** 85–94

[97] Mihokova E, Nikl M, Mares J A, Beitlerova A, Vedda A, Nejezchleb K, Blazek K and D'Ambrosio C 2006 Luminescence and scintillation properties of YAG:Ce single crystal and optical ceramics *J. Lumin.* to be published (*Proc. ICL'05, July 2005, Beijing, China*)

[98] Schmitt B, Fuchs M, Hell E, Knupfer W, Hackenschmied P and Winnacker A 2002 Structured alkali halides for medical applications *Nucl. Instrum. Methods Phys. Res.* B **191** 800–4

[99] Washida H and Sonoda T 1979 High resolution phosphor screen for x-ray image intensifier *Adv. Electron. Electron Phys.* **52** 201–7

[100] Oba K, Ito M, Yamaguchi M and Tanaka M 1988 A CsI(Na) scintillation plate with high spatial-resolution *Adv. Electron. Electron Phys.* **74** 247–55

[101] Castelli C M, Allinson N M, Moon K J and Watson D L 1994 High spatial resolution scintillator screens coupled to CCD detectors for x-ray imaging applications *Nucl. Instrum. Methods Phys. Res.* A **348** 649–53

[102] Nagarkar V V, Gupta T K, Miller S R, Klugerman Y, Squillante M R and Entine G 1988 Structured CsI(T1) scintillators for x-ray imaging applications *IEEE Trans. Nucl. Sci.* **45** 492–6

[103] Srolowitz D J, Mazor A and Bukiet B G 1998 Analytical and numerical modeling of columnar evolution in thin films *J. Vac. Sci. Technol.* A **6** 2371–80

[104] Johnson C B and Owen L D 1995 Image tube intensified electronic imaging *Handbook of Optics* vol 1 (New York: McGraw-Hill) pp 21.1–21.32

[105] Moy J-P 2000 Recent developments in X-ray imaging detectors *Nucl. Instrum. Methods Phys. Res.* A **442** 26–37

[106] Weber M J and Monchamp R R 1973 Luminescence of $Bi_4Ge_3O_{12}$: spectral and decay properties *J. Appl. Phys.* **44** 5495–9

[107] van Eijk C W E, Andriessen J, Dorenbos P and Visser R 1994 Ce^{3+} doped inorganic scintillators *Nucl. Instrum. Methods Phys. Res.* A **348** 546–50

[108] van Eijk C W E 2001 Inorganic-scintillator development *Nucl. Instrum. Methods. Phys. Res.* A **460** 1–14

[109] Suzuki H, Tombrello T A, Melcher C L and Schweitzer J S 1992 *Nucl. Instrum. Methods Phys. Res.* A **320** 263–72

[110] Dorenbos P, van Eijk C W E, Bos A J J and Melcher C L 1994 Thermoluminescence and scintillation properties of Lu_2SiO_5:Ce *J. Lumin.* **60, 61** 979–82

[111] Melcher C L, Spurrier M A, Eriksson L, Eriksson M, Schmand M, Givens G, Terry R, Homant T and Nutt R 2003 Advances in the scintillation performance of LSO:Ce single crystals *IEEE Trans. Nucl. Sci.* **50** 762–6

[112] Szupryczynski P, Melcher C L, Spurrier M A, Maskarinec M P, Carey A A, Wojtowicz A J, Drozdowski W, Wisniewski D and Nutt R 2004 Thermoluminescence and scintillation properties of rare earth oxyorthosilicate scintillators *IEEE Trans. Nucl. Sci.* **51** 1103–10

[113] Ishibashi H, Shimizu K, Susa K and Kubota S 1989 Cerium doped GSO scintillator and its application to position sensitive detectors *IEEE Trans. Nucl. Sci.* **36** 170–2

[114] Kamae T, Fukazawa Y, Isobe N, Kokubun M, Kubota A, Osone S, Takahashi T, Tsuchida N and Ishibashi H 2002 Improvement on the light yield of a high-*Z* inorganic scintillator GSO(Ce) *Nucl. Instrum. Methods Phys. Res.* A **490** 456–64

[115] Shimura N, Kamada M, Gunji A, Usui T, Kurashige K, Ishibashi H, Senguttuvan N, Shimizu S and Murayama H 2004 Zr-doped GSO:Ce single crystals and its scintillation performance *Proc. IEEE 2004 NSS-MIC (Rome, October 2004)* p 150 (M2–405, Book of Abstracts)

[116] Pauwels D, Le Masson N, Viana B, Kahn-Harari A, van Loef E V, Dorenbos P and van Eijk C W E 2000 A novel inorganic scintillator: $Lu_2Si_2O_7:Ce^{3+}$ (LPS) *IEEE Trans. Nucl. Sci.* **47** 1787–90

[117] Baryshevski V G, Kondratyev D M, Korzhik M V, Fyodorov A A, Moroz V I, Kachanov B I and Minkov B I 1993 Prospects of production of fast scintillators based on doped compound structure oxides for electromagnetic calorimeters *Nucl. Tracks Radiat. Meas.* **21** 111–2

[118] Moses W W, Derenzo S E, Fyodorov A, Korzhik M, Gektin A, Minkov B and Aslanov V 1995 $LuAlO_3$-Ce—a high-density, high-speed scintillator for gamma-detection *IEEE Trans. Nucl. Sci.* **42** 275–9

[119] Mares J, Nikl M, Chval J, Dafinei I, Lecoq P and Kvapil J 1995 Fluorescence and scintillation properties of $LuAlO_3$:Ce crystal *Chem. Phys. Lett.* **241** 311–6

[120] Lempicki A, Randles M H, Wisniewski D, Balcerzyk M, Brecher C and Wojtowicz A J 1995 $LuAlO_3$-Ce and other aluminate scintillators *IEEE Trans. Nucl. Sci.* **42** 280–4

[121] Dujardin C, Pedrini C, Gacon J C, Petrosyan A G, Belsky A N and Vasil'ev A N 1997 Luminescence properties and scintillation mechanisms of cerium- and praseodymium-doped lutetium orthoaluminate *J. Phys.: Condens. Matter* **9** 5229–43

[122] Petrosyan A G, Shirinyan G O, Ovanesyan K L, Pédrini C, Dujardin C, Garnier N, Sowinski S, Lecoq P and Belsky A 2002 Potential of existing growth methods of LuAP and related scintillators *Nucl. Instrum. Methods Phys. Res.* A **486** 74–8

[123] Chval J *et al* 2000 Development of new mixed $Lu_x(RE^{3+}_{1-x}AlO_3$:Ce scintillators ($RE^{3+} = Y^{3+}$ or Gd^{3+}): comparison with other Ce-doped or intrinsic scintillating crystals *Nucl. Instrum. Methods Phys. Res.* A **443** 331–41

[124] Petrosyan A G, Shirinyan G O, Ovanesyan K L, Pedrini C and Dujardin C 1999 Bridgman single crystal growth of Ce-doped $(Lu_{1-x}Y_x)AlO_3$ *J. Cryst. Growth* **198, 199** 492–6

[125] Kuntner C, Auffray E, Bellotto D, Dujardin C, Grumbach N, Kamenskikh I A, Lecoq P, Mojzisova H, Pedrini C and Schneegans M 2005 Advances in the scintillation performance of LuYAP:Ce single crystals *Nucl. Instrum. Methods Phys. Res.* A **537** 295–301

[126] Vedda A, Martini M, di Martino D, Laguta V V, Nikl M, Mihokova E, Rosa J, Nejezchleb K and Blazek K 2002 Defect states in $Lu_3Al_5O_{12}$:Ce crystals *Radiat. Eff. Defects Solids* **157** 1003–8

[127] Nikl M, Mihokova E, Mares J A, Vedda A, Martini M, Nejezchleb K and Blazek K 2000 Traps and timing characteristics of LuAG:Ce^{3+} scintillator *Phys. Status Solidi* b **181** R10–2

[128] Mares J A, Beitlerova A, Nikl M, Solovieva N, D'Ambrosio C, Blazek K, Maly P, Nejezchleb K and de Notaristefani F 2004 Scintillation response of Ce-doped or intrinsic scintillating crystals in the range up to 1 MeV *Radiat. Meas.* **38** 353–7

[129] Zorenko Yu, Konstankevych I, Globus M, Grinyov B and Lyubinskiy V 2003 New scintillation detectors based on oxide single crystal films for biological microtomography *Nucl. Instrum. Methods Phys. Res.* A **505** 93–6

[130] Ryskin N N, Dorenbos P, van Eijk C W E and Batygov S Kh 1994 Scintillation properties of $Lu_3Al_{5-x}Sc_xO_{12}$ crystals *J. Phys.: Condens. Matter* **6** 10423–34

[131] Zorenko Yu, Gorbenko V, Konstankevych I, Grinev B and Globus M 2002 Scintillation properties of $Lu_3Al_5O_{12}$:Ce single-crystalline films *Nucl. Instrum. Methods Phys. Res.* A **486** 309–14

[132] van Loef E V D, Dorenbos P, van Eijk C W E, Kramer K and Gudel H U 2000 High-energy-resolution scintillator: Ce^{3+} activated $LaCl_3$ *Appl. Phys. Lett.* **77** 1467–8

[133] van Loef E V D, Dorenbos P, van Eijk C W E, Kramer K and Gudel H U 2001 High-energy-resolution scintillator: Ce^{3+} activated $LaBr_3$ *Appl. Phys. Lett.* **79** 1573–5

[134] van Loef E V D, Dorenbos P and van Eijk C W E 2003 The scintillation mechanism in $LaCl_3$:Ce^{3+} *J. Phys.: Condens. Matter* **15** 1367–75

[135] Dorenbos P 2005 Scintillation mechanisms in Ce^{3+} doped halide scintillators *Phys. Status Solidi* a **202** 195–200

[136] van Loef E V D, Dorenbos P, van Eijk C W E, Kramer K W and Gudel H U 2005 Scintillation properties of K_2LaX_5:Ce^{3+} (X = Cl, Br, I) *Nucl. Instrum. Methods Phys. Res.* A **537** 232–6

[137] Annenkov A, Borisevitch A, Hofstaetter A, Korzhik M, Ligun V, Lecoq P, Missevitch O, Novotny R and Peigneux J P 2000 Improved light yield of lead tungstate scintillators *Nucl. Instrum. Methods Phys. Res.* A **450** 71–4

[138] Nikl M, Bohacek P, Vedda A, Martini M, Pazzi G P, Fabeni P and Kobayashi M 2000 Efficient medium-speed $PbWO_4$:Mo,Y scintillator. *Phys. Status Solidi* a **182** R3–5

[139] Nikl M, Bohacek P, Mihokova E, Solovieva N, Vedda A, Martini M, Pazzi G P, Fabeni P and Kobayashi M 2002 Complete characterization of doubly doped $PbWO_4$:Mo,Y scintillators. *J. Appl. Phys.* **91** 2791–7

[140] Nikl M, Bohacek P, Mihokova E, Solovieva N, Vedda A, Martini M, Pazzi G P, Fabeni P and Ishii M 2002 Enhanced efficiency of $PbWO_4$:Mo, Nb scintillator *J. Appl. Phys.* **91** 5041–4

[141] Kobayashi M, Usuki Y, Ishii M, Itoh M and Nikl M 2005 Further study on different dopings into $PbWO_4$ single crystals to increase the scintillation light yield *Nucl. Instrum. Methods Phys. Res.* A **540** 381–94

[142] Kobayashi M, Usuki Y, Ishii M and Itoh M 2005 Significant increase in fast scintillation component from $PbWO_4$ by annealing *Nucl. Instrum. Methods Phys. Res.* A **537** 312–6

[143] Mares J A, Beitlerova A, Bohacek P, Nikl M, Solovieva N and D'Ambrosio C 2005 Influence of non-stoichiometry and doping on scintillating response of $PbWO_4$ crystals *Phys. Status Solidi* c **2** 73–6

[144] Nikl M *et al* 2002 An effect of Zr^{4+} co-doping of YAP:Ce scintillator *Nucl. Instrum. Methods Phys. Res.* A **486** 250–3

[145] Morlotti R, Magro C, Vedda A, Martini M, Croci S and Nikl M 2003 The effect of co-doping by Ca^{2+}, Ta^{5+}, Sn^{4+}, and Ru^{4+} ion on the x-ray luminescent properties of Gd_2O_2S:Tb^{3+} phosphors *J. Electrochem. Soc.* **150** H81–4

[146] Nikl M, Solovieva N, Apperson K, Birch D J S and Voloshinovskii A 2005 Scintillators based on aromatic dye molecules doped in a sol–gel glass host *Appl. Phys. Lett.* **86** 101914

[147] Kandarakis I *et al* 2005 On the response of $Y_3Al_5O_{12}$:Ce (YAG:Ce) powder scintillating screens to medical imaging x-rays *Nucl. Instrum. Methods Phys. Res.* A **538** 615–30

[148] Baciero A, Placentino L, McCarthy K J, Barquero L R, Ibarra A and Zurro B 1999 Vacuum ultraviolet and x-ray luminescence efficiencies of $Y_3Al_5O_{12}$:Ce phosphor screens *J. Appl. Phys.* **85** 6790–6

[149] Flannery B P, Deckman H W, Roberge W G and D'Amico K L 1987 Three-dimensional x-ray microtomography *Science* **237** 1439–44

[150] Yasuda K, Usuda S and Gunji H 2000 Properties of a YAP powder scintillator as alpha-ray detector *Appl. Radiat. Isot.* **52** 365–8

[151] Childress N L and Miller W H 2002 MCNP analysis and optimization of a triple crystal phoswich detector *Nucl. Instrum. Methods Phys. Res.* A **490** 263–70

[152] Ryzhikov V, Gal'chinetskii L, Katrunov K, Lisetskaya E, Gavriluk V, Zelenskaya O, Starshynskiy N and Chernikov V 2005 Composite detector for mixed radiations based on CsI(Tl) and dispersions of small ZnSe(Te) crystals *Nucl. Instrum. Methods Phys. Res.* A **540** 395–402

[153] Miyata E, Miki M, Tawa N and Miyaguchi K 2005 X-ray responsivities of direct-scintillator-deposited charge coupled device *Japan. J. Appl. Phys.* **44** 1476–84

[154] Rocha J G, Ramos N F, Lanceros-Mendez S, Wolffenbuttel R F and Correia J H 2004 CMOS x-rays detector array based on scintillating light guides *Sensors Actuators* **110** 119–23

[155] Cunningham I A, Westmore M S and Fenster A 1994 A spatial-frequency dependent quantum accounting diagram and detective quantum efficiency model of signal and noise-propagation in cascaded imaging-systems *Med. Phys.* **21** 417–27

[156] Moy J P 1994 A 200 mm input field, 5–80 keV detector based on an x-ray image intensifier and CCD camera *Nucl. Instrum. Methods Phys. Res.* A **348** 641–4

[157] Ponchut C 2001 Evaluation of an x-ray imaging detector based on a CMOS camera with logarithmic response *Nucl. Instrum. Methods Phys. Res.* A **457** 270–8

[158] D'Ambrosio C and Leutz H 2003 Hybrid photon detectors *Nucl. Instrum. Methods Phys. Res.* A **501** 463–98

[159] D'Ambrosio C De, Notaristefani F, Leutz H, Puertolas D and Rosso E 2000 X-ray detection with a scintillating YAP-window hybrid photomultiplier tube *IEEE Trans. Nucl. Sci.* **47** 6–12

[160] Moszynski M, Szawlowski M, Kapusta M, Balcerzyk M and Wolski D 2000 Large area avalanche photodiodes in x-rays and light detection *IEEE Trans. Nucl. Sci.* **47** 1297–302

[161] Ikagawa T, Kataoka J, Yatsu Y, Saito T, Kuramoto Y, Kawai N, Kokubun M, Kamae T, Ishikawa Y and Kawabata N 2005 Study of large area Hamamatsu avalanche photodiode in a γ-ray scintillation detector *Nucl. Instrum. Methods Phys. Res.* A **538** 640–50

[162] Allier C P, Hollander R W, Sarro P M and van Eijk C W E 2000 Scintillator light red-out by thin photodiodes in silicon wells *Nucl. Instrum. Methods Phys. Res.* A **442** 255–8

[163] Rocha J G, Schabmueller C G J, Ramos N F, Lanceros-Mendez S, Moreira M V, Evans A G R, Wolffenbuttel R F and Correia J H 2004 Comparison between bulk micromachined and CMOS x-ray detectors *Sensors Actuators* A **115** 215–20

[164] Metzger W, Engdahl J, Rossner W, Boslau O and Kemmer J 2004 Large-area silicon drift detectors for new applications in nuclear medicine imaging *IEEE Trans. Nucl. Sci.* **51** 1631–5

[165] von Schulthess G K 2003 *Clinical Molecular Anatomic Imaging* (Philadelphia: Lippincott Williams & Wilkins)

[166] Jing T, Goodman C A, Drewery J, Cho G, Hong W S, Lee H, Kaplan S N, Mireshghi A, Perez-Mendez W and Wildermuth D 1994 Amorphous silicon pixel layers with cesium iodide converters for medical radiography *IEEE Trans. Nucl. Sci.* **41** 903–9

[167] Hermann K-P, Obenauer S, Funke M and Grabbe E H 2002 Magnification mammography: a comparison of full-field

digital mammography and screen-film mammography for the detection of simulated small masses and microcalcifications *Eur. Radiol.* **12** 2188–91
[168] Schiebel U, Conrads N, Jung N, Weibrecht M, Wieczorek H, Zaengel T, Powell M J, French I D and Glasse C 1994 Fluoroscopic x-ray imaging with amorphous silicon thin-film arrays *Medical Imaging 1994: Physics of Medical Imaging* (*Proc. SPIE* **2163**) pp 129–35
[169] Nedavnii O I and Udod V A 2001 Digital radiographic systems today—state of the art (a review) *Russ. J. Nondestr. Test.* **37** 576–91
[170] Blazek K and Tous J 2004 High resolution imaging systems for UV, x-ray and electrons Presented on *IEEE NSS-MIC, Industrial Programme (Rome, 16–22 October)*
[171] Giacconi R, Gursky H, Paolini F R and Rossi B B 1962 Evidence for x rays from sources outside the Solar system *Phys. Rev. Lett.* **9** 439–43
[172] Garmire G P, Bautz M W, Ford P G, Nousek J A and Ricker G R Jr 2003 Advanced CCD imaging spectrometer (ACIS) instrument on the Chandra X-ray Observatory *Proc. SPIE* **4851** 28–44
[173] Struder L *et al* 2001 The European photon imaging camera on XMM-Newton: the pn-CCD camera *Astron. Astrophys.* **365** L18–26
[174] Bradt H V, Swank J H and Rothschild R E 1990 The x-ray timing explorer *Adv. Space Res.* **10** 297–310
[175] Piro L, Scarsi L and Butler R C 1995 SAX: the wideband mission for x-ray astronomy *Proc. SPIE* **2517** 169–81
[176] McConnell M *et al* 2004 CASTER—a scintillator-based black hole finder probe Talk at *Beyond Einstein: from the Big Bang to Black Holes Conf. (Stanford Linear Accelerator Center, Stanford University, CA, 12–15 May 2004)*